Summer 8-18-2022

# Genetics Of Hippocampal Subregions Across Development

Jacob Pine

WASHINGTON UNIVERSITY IN ST.LOUIS
Department of Psychological & Brain Sciences

# Genetics of Hippocampal Subregions Across Development

by
Jacob Pine

A thesis presented to
The Graduate School
of Washington University in
partial fulfillment of the
requirements for the degree
of Master of Arts

August 2022
St. Louis, Missouri

# Table of Contents

# List of Figures

# List of Tables

# Acknowledgments

I would like to thank and acknowledge the following individuals who volunteered their time to help me with this project: Drs. Shelly Cooper and Josh Jackson provided support in helping me formulate the early ideas that became this project into a quantitative form. They also provided general guidance on structural equation level modeling questions; Sri Kandala provided support in helping me learn to utilize Washington University's Center for High Performance Computing Resources as well as Freesurfer processing pipelines; Drs. Arpana Agrawal and Ryan Bogdan provided structural equation modeling guidance regarding modelling conventions and interpretations that are specific to behavioral genetics applications; Dr. Jo Etzel for ensuring and teaching me best-practices for cleaning of MRI and twin-based data; and Dr. Deanna Barch. the chair of my Masters comimttee. provided supervision in all relevant domains regarding this project, including structural MRI analyses and biometric modelling, as well as study logistics, design and analyses decisions, and general encouragement. I would also like to thank Drs. Ryan Bogdan and Josh Jackson for serving as members on my Masters committee I have never worked so long on one project, and many of the skills I learned during this project I had never encountered before. Without the above individuals'

guidance and support, this project would not have been possible. Without their support, I would be a less effective and competent scientist than I am today.

Jacob Pine

*Washington University in Saint Louis*

*August 2022*

ABSTRACT OF THE THESIS

Genetics of Hippocampal Subregions Across Development

by

Jacob Pine

Master of Arts in Clinical Psychology

Washington University in St. Louis, 2022

Professor Deanna Barch

Behavioral genetic analyses have not demonstrated robust, unique, genetic correlates of hippocampal subregion volume. The following study is the first population-based investigation of a) hippocampal longitudinal axis genetic factors b) hippocampal transverse axis genetic factors using both T1 and T2 MRI images and c) differences in the genetic components of hippocampal volume between post-adolescent adults and pre-adolescent children. Twin-based biometric analyses demonstrated that longitudinal axis subregions are associated with significant, unique, genetic variance, and that longitudinal axis subregions that are closer to one another are more genetically related than those further to one another. Although our analyses find that certain transverse axis subfields have significant, unique, sources of genetic variance, others (e.g, CA1, DG) do not exhibit significant, unique, sources of genetic variance. Lastly, we do not find any differences in univariate or multivariate sources of genetic influence between children and adults. This study is the first to demonstrate evidence of genetic differentiation of gray matter volume along the human hippocampal longitudinal axis in living humans. Given that twin-based study designs are the most statistically powered to detect aggregated genetic effects, and the fact that the following study utilizes an unprecedented sample size to study the genetic components of hippocampal volume (930 twin pairs), the

following study represents the most statistically powered investigation of hippocampal genetic differentiation in living humans.

# Chapter 1

# Study Manuscript

## 1.1 Introduction

Work in rodents (Fanselow and Dong, 2010), non-human primates (Strange, Witter, Lein, and Moser, 2014) and humans (Poppenk, Evensmoen, Moscovitch, and Nadel, 2013) conclusively demonstrates that the hippocampus differs in structure, function, and connectivity along its longitudinal axis. Recent work in humans suggests that hippocampal longitudinal-axis subregions also differ in their developmental trajectories (Langnes, Sneve, Sederevicius, Amlien, Walhovd, and Fjell, 2020) and functional properties (Langnes, Vidal-Piñeiro, Sneve, Amlien, Walhovd, and Fjell, 2019) across age. Importantly, there is another dimension of heterogeneity across the hippocampus, which is commonly referred to as the hippocampal transverse axis. The hippocampal transverse axis is separated into various subfields (e.g Cornu Ammonis (CA), Dentate Gyrus (DG)), many of which also have distinct structural, functional, and connectivity properties (see Lisman, Coyle, Green, Javitt, Benes, Heckers, and Grace, 2008). The transverse axis subfields make up different relative proportions of

total hippocampal volume when moving along the hippocampal longitudinal axis, with CA subfields (CA1-3) making up a higher proportion of total volume in anterior portions of the hippocampus, and the DG making up a higher proportion in posterior regions (Malykhin, Lebel, Coupland, Wilman, and Carter, 2010).

There is a rich experimental research tradition exploring the genetic constituents of hippocampal longitudinal and transverse axis structure, however the translation of this work to the study of human individual differences is in its infancy. Experimental work suggests that there is a genetic contribution to longitudinal axis (Fanselow and Dong, 2010; Vogel et al., 2020), and transverse axis (Thompson et al., 2008; Zhao, Lein, He, Smith, Aston, and Gage, 2001) organization in the hippocampus. Population-based studies in humans, however, have not been able to reflect these findings. These population-based studies have failed to detect unique genetic correlates of hippocampal transverse axis structure (Elman et al., 2019; van der Meer et al., 2020) relative to the whole hippocampus. Recent work suggests that existing population-based magnetic resonance imaging (MRI) datasets may not have the required image quality to validly estimate the gray matter volume of transverse axis subfields (Wisse, Biessels, and Geerlings, 2014; Wisse et al., 2021). By contrast, segmentation of longitudinal axis subregions does not require the same quality of MRI data as does segmentation of the transverse axis subregions because the contours of longitudinal axis subregions are easier to detect than those of the transverse axis. No studies have investigated the genetic components of gray matter volume across the hippocampal longitudinal axis in population-based samples, although work has investigated differences in the genetics of hippocampal microstructure (T1/T2 contrast) using a population-based cohort (Bayrak, Vos de Wael, Schaare, Caldairou, Bernasconi, Bernasconi, Bernhardt, and Valk, 2021). Furthermore, studies of hippocampal genetics have typically only included adults, or instead have aggregated across age groups. However, there is reason to hypothesize that the relationship between genetic variables and

hippocampal gray matter volume may differ in degree or kind between pre-adolescent and post-adolescent individuals. Thus, the goal of the current study is to use state-of-the art methods (Iglesias et al., 2015) for automated segmentation of the hippocampus in order to generate new insights regarding the genetics of hippocampal structure. The following study will be the first twin-based heritability study to investigate: 1) the sources of variance – genetic and environmental - in gray matter along the hippocampal longitudinal axis, 2) the latent genetic factors influencing gray matter along the hippocampal transverse axis using both T1 and T2 images and 3) age-related differences in the latent genetic factors influencing hippocampal gray matter along both the longitudinal and transverse axes.

There are several lines of evidence suggesting that the genetic factors influencing gray matter volume may differ along the hippocampal longitudinal axis. Recent work using samples from post-mortem tissue in the Allen Human Brain Atlas suggests that gene expression in the hippocampus varies along a longitudinal gradient (Vogel et al., 2020). This database includes numerous tissue samples from various positions along the hippocampal longitudinal axis, and Vogel et al. demonstrated that the position of each sample along the hippocampal longitudinal axis could be predicted from a LASSO-PCR algorithm using only gene expression data (Vogel et al., 2020). Furthermore, Vogel et al. demonstrated that the most influential gene sets within this model exhibited varying degrees of transcript expression along the hippocampal longitudinal axis. Many of these gene sets are implicated in processes that determine hippocampal structure specifically (Vogel et al., 2020) which suggests that genetic variation may relate to gray matter volume in population-based samples. Other evidence for genetic differences along the hippocampal longitudinal axis comes from studies of psychopathologies with high heritability that are thought to reflect volumetric reductions in specific regions of the hippocampal longitudinal axis. Schizophrenia, for instance, has a heritability of roughly 80% (Cardno et al., 1999) and is thought to involve a deficit specifically in the anterior section

of the hippocampus (McHugo, Talati, Woodward, Armstrong, Blackford, and Heckers, 2018; McHugo, Armstrong, Roeske, Woodward, Blackford, and Heckers, 2020; Sahakyan, Meller, Evermann, Schmitt, Pfarr, Sommer, Kwapil, and Nenadić, 2021). As such, although the evidence is inconclusive regarding the genetic correlates of reduced anterior hippocampus volume in Schizophrenia, such data suggest the possibility that certain genetic factors may differentially affect one region of the hippocampal longitudinal axis, but not the other. The current study builds on this work by investigating the genetic basis of individual differences in hippocampal gray matter along the longitudinal axis.

Although there is ample evidence for genetic differences along the hippocampal transverse axis, individual differences in transverse axis volumes are more difficult to measure in humans than those from longitudinal axis volumes. Importantly, T1-weighted, $1mm^3$ volume MRI images may be insufficient to yield valid estimates of volume for transverse axis subfields (e.g CA, DG, and Subiculum) using automated methods (Wisse et al., 2021). Many large-scale MRI datasets are acquired with approximately $1mm^3$ resolution (e.g UK Biobank, Human Connectome Project-Young Adult, Adolescent Brain and Cognitive Development), and this has introduced obstacles for detecting unique genetic correlates of transverse axis subfield volume (Elman et al., 2019; van der Meer et al., 2020). Population-based studies of hippocampal genetics depend critically on the performance of automated hippocampal segmentation methods (Pipitone, Park, Winterburn, Lett, Lerch, Pruessner, Lepage, Voineskos, and Chakravarty, 2014; Iglesias et al., 2015; Yushkevich et al., 2015; Plassard, Bao, McHugo, Beason-Held, Blackford, Heckers, and Landman, 2021) to yield valid estimates of subregion volumes. When using the Freesurfer-based hippocampal segmenation algorithm, the volume estimates for many hippocampal subfields are driven heavily by a priori predictions when only T1, $1mm^3$ MRI images are utilized (see online documentation for tool from (Iglesias et al., 2015), which may account for the difficulty of detecting unique genetic correlates of transverse axis subfields.

Updates to the Freesurfer-based hippocampal segmentation tool, however, now allow for the combination of multiple MRI images (e.g. T1 and T2), and this capability has not yet been employed to study the genetic correlates of hippocampal subregions. Thus, although prior studies found that T1, $1mm^3$ isotropic images were unable to detect unique genetic correlates of hippocampal transverse axis volume (Elman et al., 2019), these effects may be detected when using a combination of T1 and T2 images in samples of sufficient size. Furthermore, the Freesurfer hippocampal segmentation tool is now capable of segmenting the hippocampus into longitudinal-axis subregions, which, as previously mentioned, do not have the same validity concerns as transverse axis subfields at $1mm^3$ resolution (Wisse et al., 2021).

Lastly, existing work on the genetics of the hippocampus suggests that the genetic architecture of hippocampal volume may differ between children and adults. Genome Wide Association Studies (GWAS) of hippocampal gray matter volume demonstrate statistically significant effects for SNPs related to oxidative stress and glucocorticoid-mediated activity in the hippocampus (van der Meer et al., 2020), and for gene-sets related to sexual reproduction and gamete generation (Bahrami, Nordengen, Shadrin, Frei, Meer, Dale, Westlye, Andreassen, and Kaufmann, 2021). Humans reach sexual maturity during adolescence, and this developmental period also comes with significant increases in psychosocial stress (Blakemore and Choudhury, 2006). Thus, pre-adolescent children have yet to experience the neurobiological phenomena that may partially mediate the relationship between genetic variability and individual differences in hippocampal volume. This may lead to potentially significant differences in the genetic constituents of hippocampal volume between pre-adolescent children and post-adolescent adults. Age-related changes in heritability have been demonstrated for many behavioral phenotypes (e.g body-mass index, intelligence quotient), although this phenomenon is less robust with neuroimaging studies perhaps due to the difficulty of collecting large samples (for examples see Batouli, Trollor, Wen, and Sachdev, 2014; Swagerman,

Brouwer, de Geus, Hulshoff Pol, and Boomsma, 2014; Le Grand et al., 2021). Age-related differences in the heritability of behavioral phenotypes have been interpreted as evidence of the influence of gene-by-environment interactions (Beam and Turkheimer, 2013; Briley and Tucker-Drob, 2017) and age-related differences in gene expression (Bouchard, 2013). As the hippocampus is both highly sensitive to the environment (Maguire, Gadian, Johnsrude, Good, Ashburner, Frackowiak, and Frith, 2000; Maguire, Woollett, and Spiers, 2006; McEwen, 2012) and highly heritable (Eyler et al., 2011; Patel, Park, Devenyi, Patel, Masellis, Knight, and Chakravarty, 2017; Elman et al., 2019), it is reasonable to hypothesize that gene-by-environment interactions may produce age-related changes in the heritability of hippocampal volume. Adolescence has also been shown to involve changes in neurotransmitter availability in hippocampal circuits, which may indicate that the genetic correlates of hippocampal volume may exhibit developmental changes in expression (Lavenex, Sugden, Davis, Gregg, and Lavenex, 2011). In summary, there is ample evidence to suggest that there may be age-related differences in the heritability of hippocampal volume, although this phenomenon has been difficult to uncover in extant neuroimaging data.

The following study will utilize data collected from two population-based studies of monozygotic (MZ) and dizygotic (DZ) twins: the Adolescent Brain and Cognitive Development (ABCD; baseline sample; 381 MZ and 436 DZ pairs) study and the Human Connectome Project – Young Adult (HCP; 138 MZ and 79 DZ pairs) sample in order to investigate three primary aims. First, this study will investigate differences in the magnitude of genetic influence across the hippocampal longitudinal axis subregions, and will also investigate common and unique sources of genetic variance across hippocampal longitudinal axis subregions. Differences in the magnitude of genetic influence will be investigated using univariate twin-based genetic models, while sources of correlated and subregion-specific genetic variation across hippocampal subregions will be investigated using multivariate twin-based genetic

models. Secondly, this study will investigate unique genetic factors influencing hippocampal transverse axis subfield volume with T1 and T2 images combined in order to investigate whether a combination of T1 and T2 MRI scans can facilitate the detection of unique sources of genetic variance for hippocampal transverse axis subfields. Bivariate twin-based heritability models will be used to determine whether there are significant sources of genetic variation for individual transverse axis subfields after accounting for shared sources of genetic variance with total hippocampal volume. Lastly, this study will investigate whether there are differences in the heritability of hippocampal longitudinal axis volume between pre-adolescent children in the ABCD sample, and post-adolescent adults in the HCP sample. Significant differences between these two samples will be assessed by investigating the confidence interval estimates for parameters from the univariate and multivariate models. These three aims represent important gaps in current knowledge of genetic influences on the human hippocampus; given that twin-based studies are the most statistically powered design to detect aggregated genetic effects, and the fact that the following study utilizes an unprecedented sample size to study the genetic components of hippocampal volume in living humans (930 twin pairs), the following study represents the most statistically-powered investigation of these existing knowledge gaps to date.

## 1.2 Results

### 1.2.1 Aim 1: Genetic contributions to Long Axis Subregion Volume

Based on univariate ACE/ADE model output, there were no significant differences in the magnitude of heritability across hippocampal longitudinal axis subregions. Univariate model output is displayed in Table 1. In the ABCD sample, there was a qualitative trend for greater heritability at more posterior regions of the hippocampus, with the hippocampal tail

being the most heritable and the hippocampal head being the least heritable. In the HCP sample, there was a qualitative trend in the opposite direction, with greater heritability at more anterior regions of the hippocampus. None of these differences across subregions were statistically significant in either sample.

Table 1.1: Univariate variance components for longitudinal axis subregions from ABCD and HCP samples

| Sample | Subregion | $DZ_r$ | $MZ_r$ | Heritability ($h^2$) | Common Environment ($c$) | Unique Environment ($e$) |
|---|---|---|---|---|---|---|
| ABCD | Head | 0.50 | 0.87 | 0.76 (0.63-0.89) | 0.11 (0.00-0.24) | 0.12 (0.10-0.15) |
| | Body | 0.42 | 0.80 | 0.78 (0.63-0.84) | 0.03 (0.00-0.17) | 0.19 (0.16-0.23) |
| | Tail* | 0.34 | 0.80 | 0.80 (0.76-0.83) | NA (NA-NA) | 0.20 (0.17-0.24) |
| | Whole | 0.48 | 0.88 | 0.80 (0.67-0.90) | 0.07 (0.00-0.21) | 0.12 (0.10-0.14) |
| HCP | Head | 0.47 | 0.91 | 0.87 (0.59-0.93) | 0.04 (0-0.32) | 0.09 (0.07-0.12) |
| | Body* | 0.37 | 0.87 | 0.86 (0.82-0.89) | NA (NA-NA) | 0.14 (0.11-0.18) |
| | Tail* | 0.42 | 0.82 | 0.83 (0.77-0.87) | NA (NA-NA) | 0.17 (0.13-0.23) |
| | Whole | 0.44 | 0.92 | 0.92 (0.64-0.94) | 0.00 (0.00-0.28) | 0.08 (0.06-0.10) |

*Note*: Asterisk (*) indicates ADE model used instead of ACE.

Although the magnitude of genetic effects did not differ between longitudinal axis subregions, multivariate models suggested that gray matter volumes of the hippocampal head, body, and tail, were partially associated with unique sources of genetic variance that did not contribute to other hippocampal longitudinal axis subregions. These results are depicted in Figure 1. Path coefficients from the final genetic Cholesky factors were standardized and squared. The path coefficient for the final genetic Cholesky factor ($a_{33}$ from latent variable $A_3$ in figure 1B) achieved statistical significance for each longitudinal axis subregion in the ABCD sample (head $a_{33} = 0.31$ [0.27-0.35]; body $a_{33} = 0.20$ [0.17-0.24]) ; tail $a_{33} = 0.43$ [0.38-0.48]). The estimates for the residual genetic variances of the hippocampal head, body, and tail were similar in the HCP sample (head $a_{33} = 0.37$ [0.29-0.46]; body $a_{33} = 0.20$ [0.15-0.26]; tail $a_{33} = 0.37$ [0.29-0.46]), and each were statistically significant.

While the final genetic factor of the Cholesky decomposition ($A_3$) represents the degree of unique genetic variance for an individual subregion, the second factor from the model

($A_2$) represents the degree of common genetic variance that remains after accounting for the influence of a single subregion (e.g., the common genetic variance between the hippocampal head and tail after accounting for shared genetic influence with the hippocampal body). The estimated effects of the second factor were statistically significant for all subregions and in both samples. This suggests that all pairs of subregions share common genetic variance not shared with the third subregion, and that no one hippocampal subregion accounts for the total effect of genetic influences across the hippocampal longitudinal axis.

Path estimates from the multivariate Cholesky decomposition were also converted to genetic correlations, which represent shared sources of genetic variance across pairs of variables. Genetic correlations were computed by multiplying the genetic covariance of the two subregions divided by the square root of the product of their genetic variance. The genetic correlations were statistically significant between all pairs of hippocampal longitudinal axis subregions. Interestingly, however, the magnitude of the genetic correlations varied as a function of distance along the hippocampal longitudinal axis. In other words, although we found evidence for significant genetic overlap between the hippocampal head, body, and tail, hippocampal subregions that were further apart from one another on the longitudinal axis were less genetically related to each other than regions that were closer to one another. The hippocampal head and hippocampal tail shared the lowest amount of genetic variance in both the HCP ($r_A$ = 0.38 [0.28-0.49]) and ABCD ($r_A$ = 0.48 [0.42-0.54]) samples. In both samples the genetic correlations between the hippocampal head and hippocampal tail were significantly lower than the genetic correlations between the hippocampal head and the hippocampal body (HCP: $r_A$ = 0.74 [0.67-0.80]; ABCD: $r_A$ = 0.80 [0.77-0.83]) and the hippocampal body and the hippocampal tail (HCP: $r_A$ = 0.71 [0.63-0.78]; ABCD: $r_A$ = 0.67 [0.62-0.72]).

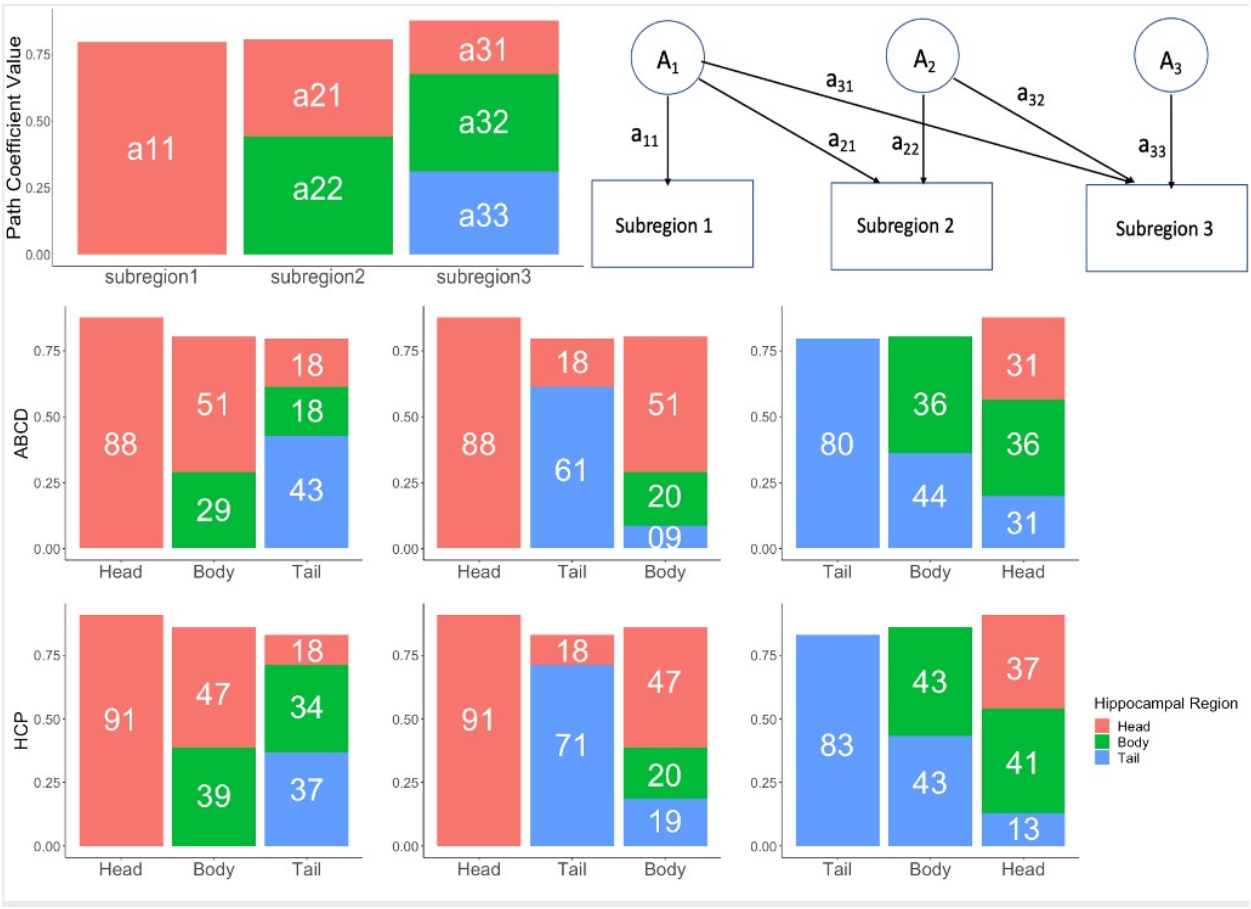


Figure 1.1: Multivariate Cholesky Path Results

1A and 1B: Additive genetic effects from the trivariate cholesky are displayed visually in figure 1B. Each of the path estimates (e.g a33) from the latent factors (e.g A3, A2) in figure 1B correspond to a color-coded bar in figure 1A. Each latent factor from 1B is represented by a specific, color-coded bar in 1A (e.g in this template, coefficients from $A_1$, which prioritizes variance in "subregion 1", are represented in red in 1A). The total, univariate, additive genetic effect for each subregion (organized along the x-axis in figure 1A) is represented by the total, color-independent, height of the bar (e.g in 1A, the univariate, additive genetic effect on "subregion 3" is around 0.80, and is the sum of the red, green, and blue bars). 1C: Triavriate cholesky coefficients for the ABCD dataset are demonstrated on the top row, while coefficients for the HCP dataset are displayed on the bottom row. While the templates from 1A and 1B can be thought of as representing raw coefficient estimates, the metrics shown in 1C (and reported in the results section) are derived by standardizing the additive-genetic variance/covariance matrix (i.e dividing it by the phenotypic variance/covariance matrix), and then multiplying the resulting matrix by itself. This operation is necessary in order to interpret the coefficients from the Cholesky model as partitioned sources of shared and unique genetic influence on the overall, univariate, heritability of a given hippocampal subregion. Unique genetic effects are shown in 1C on the rightmost subregion in each bar graph, and correspond to a specific color-coded bar. For instance, in the left-most bar graphs from 1C, the unique genetic effects on the hippocampal tail are represented by the values in the blue bars. The legend in the bottom right demonstrates that blue bars represent genetic effects that correspond to the latent genetic factor that represents variance primarily associated with the hippocampal tail. As the blue bars in these specific bar graphs do not contribute to the total, univariate, genetic effect for any other subregion, we can think of the blue bars as unique genetic effects.

Notably, in both samples, the 95% confidence intervals for the genetic correlations between the head and tail did not overlap with the 95% confidence intervals for the genetic correlations between the body and tail or the head and body. This suggests that the genetic factors influencing proximal regions on the hippocampal longitudinal axis are, statistically speaking, significantly more similar to one another than the genetic factors influencing distal regions. The above analyses were conducted as bivariate AE models, however the same pattern of statistical significance was also evident in bivariate ACE models.

### 1.2.2 Aim 2: Genetic Contribution to Transverse Axis Subregion Volume

Unique sources of genetic variability across the hippocampal transverse axis were analyzed using bivariate Cholesky decompositions and genetic correlations. The bivariate Cholesky model can be visually conceptualized as a bivariate version of the model illustrated in Figure 1B. In order to investigate unique sources of genetic variance associated with each transverse axis subfield, the whole hippocampus was represented by "subregion 1" in the model, each specific hippocampal transverse axis subfield was represented by "subregion 2," and the unique genetic variance associated with each hippocampal transverse axis subfield, beyond total hippocampal volume, was represented by path coefficient "$a_{22}$."

The unique genetic variances associated with each transverse axis subfield are displayed in Table 2 for both the ABCD and HCP samples. In short, genetic factors unique to each transverse axis subfield ranged from 0.02 (Hippocampal Fissure) to 0.35 (Parasubiculum) in HCP, with only six subfields showing statistically significant evidence for unique genetic variance beyond total hippocampal volume. For ABCD, estimates of unique genetic variance were somewhat higher (range: 0.07 – 0.43) but the confidence intervals for the residual genetic

Table 1.2: Unique genetic variances ($a_{22}$) for transverse axis subfields after accounting for shared genetics with total hippocampus

| Transverse Subfield | HCP | ABCD | Combined | Reduced ABCD |
|---|---|---|---|---|
| Subiculum | 0.18 (0.07-0.24) | 0.26 (0.19-0.30) | 0.25 (0.19-0.28) | 0.01 (0.00-0.24) |
| CA1 | 0.09 (0.03-0.14) | 0.07 (0.04-0.11) | 0.08 (0.05-0.11) | 0.10 (0.01-0.26) |
| Fissure | 0.02 (0.00-0.30) | 0.29 (0.08-0.44) | 0.32 (0.14-0.43) | 0.00 (0.00-0.46) |
| Presubiculum | 0.17 (0.00-0.32) | 0.21 (0.13-0.27) | 0.21 (0.13-0.27) | 0.26 (0.11-0.33) |
| Parasubiculum | 0.35 (0.08-0.54) | 0.39 (0.28-0.45) | 0.40 (0.32-0.46) | 0.40 (0.22-0.50) |
| GC-ML-DG | 0.10 (0.04-0.14) | 0.12 (0.07-0.17) | 0.13 (0.08-0.18) | 0.27 (0.07-0.36) |
| CA3 | 0.29 (0.12-0.38) | 0.23 (0.14-0.28) | 0.25 (0.17-0.29) | 0.22 (0.00-0.30) |
| CA4 | 0.09 (0.03-0.14) | 0.12 (0.07-0.17) | 0.13 (0.08-0.17) | 0.26 (0.08-0.33) |
| Fimbria | 0.26 (0.00-0.45) | 0.38 (0.22-0.46) | 0.37 (0.23-0.44) | 0.00 (0.00-0.22) |
| HATA | 0.04 (0.00-0.24) | 0.43 (0.29-0.50) | 0.39 (0.26-0.47) | 0.46 (0.04-0.59) |

*Note*: GC-ML-DG = Granule Cell-Molecular Layer-Dentate Gyrus;
HATA = Hippocampal-Amygdala-Transition-Area

variance of nearly every transverse axis subfield overlapped between the HCP and ABCD sample. As a result, follow-up analyses were conducted using a combined sample. These combined analyses indicate that there is statistically significant evidence for unique genetic influences on all transverse axis subfields. Nevertheless, certain regions (e.g CA1, CA4, GC-ML-DG) have unique genetic effects that are quite low. Furthermore, the confidence intervals for the unique genetic estimates of these regions remain virtually unchanged independent of sample size. Further analyses were conducted using a randomly sampled ABCD dataset of reduced size, with the same number of MZ and DZ twins as the HCP dataset. These analyses were conducted in order to assess whether the use of T1/T2 combined scans or whether larger sample size led to more statistically significant unique genetic effects for transverse axis subfields in the ABCD dataset. Only one transverse axis subfield yielded a statistically significant unique genetic effect, which suggests that the differences in statistical significance for transverse axis subfields between the HCP and ABCD samples are likely driven by the influence of sample size.

### 1.2.3 Aim 3: Genetic Contributions to Hippocampal Subregions across Development

The heritability of hippocampal volumes was qualitatively lower in the ABCD sample relative to the HCP sample, however these differences were not statistically significant (see Table 1). In addition, there were no readily discernible differences in the pattern of genetic correlations among hippocampal longitudinal axis subregions between the ABCD and HCP samples (see Figure 2 and supplementary materials). These findings suggest that there are negligible, if any, differences in the genetics of hippocampal subregion volumes between the ABCD and HCP samples. Bivariate genetic correlations among all hippocampal longitudinal and transverse axis subregions are displayed in Figure 2 for both samples, which demonstrates the broad correspondence in hippocampal genetic architecture between these two samples. Unique environmental correlations and phenotypic correlations are displayed similarly in the supplemental materials.

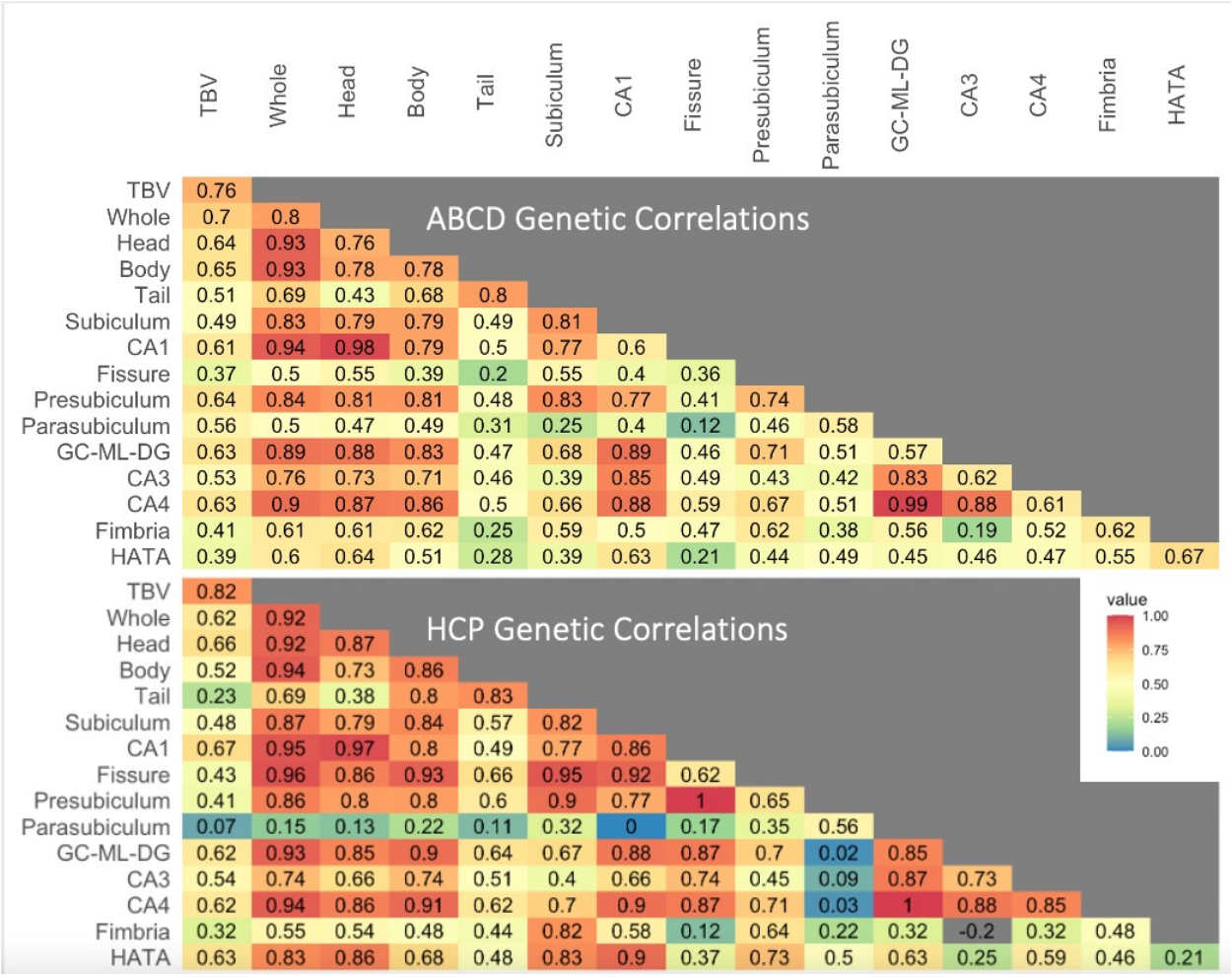


Figure 1.2: Genetic correlation heat maps

Genetic correlations for both ABCD and HCP samples. Univariate additive genetic effects are plotted on the diagonal

## 1.3 Discussion

In summary, this study provides evidence that individual differences in hippocampal gray matter volume are related to different genetic factors depending on the tissue's position along the longitudinal axis. Multivariate Cholesky models demonstrated that there is statistically significant residual genetic variance associated with the hippocampal head,

body, and tail, which remains after accounting for shared sources of genetic variance across all three subregions. Multivariate Cholesky models also demonstrated significant sources of common genetic variance across the hippocampal head, body, and tail. The genetic correlations extracted from multivariate Cholesky models demonstrate that the degree of common genetic variance between these regions depends on their proximity to one another along the hippocampal longitudinal axis. In other words, hippocampal subregions that are closer to one another along the longitudinal axis are more genetically related to one another than subregions that are further from one another along this axis. In addition, this study demonstrates that the use of T1 and T2 combined hippocampal segmentations are unable to detect unique genetic sources of variance of gray matter volume in several hippocampal transverse axis subfields, such as CA1 and the Dentate Gyrus (represented by the Granule Cell – Molecular Layer – Dentate Gyrus [GC-ML-DG]). This study's results also suggest, however, that unique sources of genetic variance are detectable for several other hippocampal transverse axis subfields when using samples of sufficient size. Finally, this study does not find any differences in the magnitude of the genetic effect for hippocampal longitudinal axis subregions across age cohorts.

This study suggests that there are unique genetic sources of variance in gray matter volume across hippocampal longitudinal axis subregions. Importantly, our findings cannot be explained by differences in the measurement properties of hippocampal longitudinal axis subregions. Previous work has demonstrated that the reliabilities of gray matter volume estimates for the hippocampal head, body, and tail are virtually identical when using Freesurfer-based automated segmentation algorithms (Kahhale, Buser, Madan, and Hanson, 2021; Seiger et al., 2021). It is therefore unlikely that the statistical effects from trivariate models are the result of differential susceptibility to measurement error across hippocampal longitudinal axis subregions. Furthermore, measurement error is captured by factors related to unique

environmental experiences not heritability, so if volume estimates for one hippocampal region were more susceptible to noise than those for another hippocampal region we would see significant differences in heritability estimates for these regions. In contrast with this hypothetical scenario, however, there were no significant differences in heritability across hippocampal subregions. Lastly, although there are differences in the size of each hippocampal longitudinal axis subregion, our findings cannot be explained by the effects of region size. The genetic correlation between the hippocampal body, which was intermediate in size, and the hippocampal tail, which was the smallest in size, was significantly greater than the genetic correlation between the hippocampal head, which was largest in size, and the hippocampal tail. These effects are inconsistent with the interpretation that region size is associated with the magnitude of genetic correlation. Ultimately, this study is the first to demonstrate genetic differences across the hippocampal longitudinal axis in a population-based cohort. This study's results confirm the extensive genetic analyses conducted in rodents and post-mortem human tissue.

Bivariate analyses of hippocampal transverse axis subfields suggest that there are statistically significant unique genetic sources of variance of gray matter volume in many of these regions. Previous work has found that the residual genetic variances associated with hippocampal transverse axis subfields are quite low and often statistically nonsignificant after accounting for shared genetic variance associated with the total hippocampus (Elman et al., 2019). These findings have been considered unexpected given existing knowledge on hippocampal transverse axis subfields, and as a result have been cited as evidence that automated hippocampal transverse axis segmentations are invalid for $1mm^3$ MRI images (Wisse et al., 2021). It has been noted that Freesurfer's segmentation of many hippocampal transverse axis structures are driven heavily by a priori expectations at $1mm^3$ resolution, and that, as a result, automated segmentations of gray matter using these images may often represent a proxy measure of

total hippocampal gray matter rather than subfield-specific gray matter (Iglesias et al., 2015; Wisse et al., 2021). While this is a significant threat to the validity of $1mm^3$ resolution segmentations, the results of the current study suggest that the unique genetic variances of a number of transverse axis subfields are detectable given twin-based study designs of sufficient sample sizes, as in the ABCD study. In other words, while a priori expectations may still heavily contribute to many of Freesurfer's transverse axis segmentations, sufficiently powered samples may be able to overcome the influence of the algorithm's prior on estimates of residual genetic variance. At the same time, however, the estimates for the residual genetic variances of several hippocampal transverse axis subfields, including CA1, CA4, and GC-ML-DG, suggest that these regions do not clearly demonstrate unique genetic variance. The residual genetic variance estimates for these regions were quite low, and the confidence intervals for these estimates essentially did not change even when increasing the size of the sample considerably. The residual genetic variances for CA1, CA4, and the GC-ML-DG are consistent with the proposal that gray matter estimates for these regions are driven primarily by a priori expectations rather than the empirical data. It has been noted that automated segmentations of the CA1 and Dentate Gyrus, in particular, are fraught when using $1mm^3$ resolution due to difficulties detecting the contours that separate these regions. Thus, our data suggests that the automated segmentation output for gray matter of the CA1 and Dentate Gyrus regions may be invalid at insufficient image resolution.

This study did not find any statistically significant differences in the magnitude of heritability or genetic correlations among hippocampal longitudinal axis subregions between the child and adult samples. This provides modest evidence that genetic variation contributes to hippocampal longitudinal axis subregion volume to a similar degree in pre-adolescent children and post-adolescent adults. As this was a between-subjects design, however, these findings can only provide relatively weak information regarding the sources hippocampal genetic

variability between children and adults. Age-related changes in the heritability of phenotypes are theoretically dependent on the timing and duration of the mechanisms that generate the expression of the phenotype. Thus, the lack of difference in heritability between the children and adults may reflect the fact that the mechanisms that account for hippocampal volume in the general population have mostly completed by late childhood. While some epidemiological studies have suggested that sexual maturation and adolescence may be part of the mechanisms that determine individual differences in hippocampal volume, a great deal of work suggests that hippocampal volume may be relatively stable from around late childhood and onward (Lavenex and Banta Lavenex, 2013). Thus, we may need to examine even younger samples to detect age related differences in either the magnitude of heritability or the patterns of shared genetic variance. Further, adolescence and young adulthood has been shown to be a dynamic period of white matter change in the hippocampus, and age-related changes in the functional properties of the hippocampus have also been shown across development (Langnes, Vidal-Piñeiro, Sneve, Amlien, Walhovd, and Fjell, 2019; Conley, Skalaban, Rapuano, Gonzalez, Laird, Dick, Sutherland, Watts, and Casey, 2021). Thus, age-related changes in the genetic correlates of hippocampal properties may be more readily observed for other features of the hippocampus, like white-matter and BOLD response, rather than gray matter volume.

This study had several limitations. First, gray matter along the hippocampal longitudinal axis was separated into three discrete subregions. While existing work demonstrates the validity of these subregions, other work suggests that hippocampal longitudinal axis heterogeneity is expressed continuously rather than discretely (Vogel et al., 2020). Thus, our segmentation of hippocampal gray matter into discrete longitudinal axis subregions may have biased our results. Secondly, this study investigated age-related differences in the heritability of hippocampal subregions using a between-subjects design. A within-subjects design would likely provide a more sensitive exploration of age-related differences in hippocampal genetics, as this design

would allow us to test the degree to which the genetic components of hippocampal gray matter are related to one another throughout adolescent development. Third, while this study provides the largest twin-based study of hippocampal genetics, our sample size was nevertheless underpowered to detect the effects of the common environment. Lastly, the age range of our sample size may not have been optimal for detecting developmental differences in the heritability of hippocampal gray matter volume. The child sample for our study comprised children ages 9-11, and the adult sample for our study comprised adults 22-36. Thus, our study was best able to detect changes in the heritability of hippocampal gray matter volume associated with adolescent development. Existing work suggests, however, that hippocampal gray matter volume is relatively stable throughout adolescence, and undergoes more dynamic changes in early-to-middle childhood (Insausti, Cebada-Sánchez, and Marcos, 2010; Lavenex and Banta Lavenex, 2013). Thus, if we had an even younger sample, we might see more evidence of age-related differences in the degree of unique versus shared genetic variance in hippocampal subregions.

This study provides evidence that genetic heterogeneity along the hippocampal longitudinal axis is evident in gray matter measurements from human, population-based, samples. This genetic heterogeneity is evident in the statistical significance of estimates of residual genetic variance estimates of individual longitudinal axis subregions, and the statistical significance of comparisons between bivariate genetic correlations among longitudinal axis subregions. The collection of univariate and multivariate analyses conducted as part of this study suggests that these statistical effects are driven by substantive genetic differences between hippocampal longitudinal axis subregions, and are not likely driven by spurious sources of variation. While existing work has demonstrated genetic differences along the hippocampal longitudinal axis in rodents and human post-mortem tissue, this is the first study to demonstrate genetic differences in a human population-based sample. Furthermore, this study adds to ongoing

efforts to optimize the use of automated hippocampal transverse-axis segmentations by demonstrating that unique sources of genetic variance can be detected for certain subfields, but not for others. This study's results suggest that these genetic effects can only be demonstrated with relatively large samples of twins. Consequently, this study's results speak to the difficulty of detecting unique sources of genetic variance in GWAS settings, which are underpowered relative to twin-based analyses.

## 1.4 Materials and Methods

### 1.4.1 Participants

The sample of children used for this study was comprised of participants within the Adolescent Brain and Cognitive Development (ABCD) (ABCD Twin hub; Iacono, Heath, Hewitt, Neale, Banich, Luciana, Madden, Barch, and Bjork, 2018). The sample of adults used for this study was comprised of MZ and DZ twin pairs within the WU-Minn Human Connectome Project (S-1200 release) (HCP; Van Essen, Smith, Barch, Behrens, Yacoub, Ugurbil, and WU-Minn HCP Consortium, 2013). Twin pairs from both samples were recruited using the respective birth registries for the years 2006-2008 for each state. This study only utilized data from twin pairs with genotype-confirmed zygosity status. The final sample for this study consisted of 910 twin pairs: the child sample analyzed for this study consisted of 713 twin pairs (Monozygotic (MZ) = 310; Dizygotic (DZ) = 403), and the adult sample consisted of 217 (MZ = 138; DZ = 79). Of the entire sample, 47 twin pairs did not have matching sex (all in ABCD sample), however, our results did not change whether we excluded these individuals or not. The average age of the ABCD sample was 10.1 years, and ranged from 9-10.9 years old. The average age of the HCP sample was 29.3 years old, and ranged from 22-36 years old. Of the entire ABCD sample, 376 pairs identified as White, 112 identified as Black, 136

identified as Hispanic, 18 identified as Asian, and 70 as a race different than those just listed. One twin pair did not know or did not report their race. Of the entire HCP sample, 182 pairs identified as White, 22 identified as Black, 8 identified as Asian/Native Hawaiian/or Pacific Islander, 3 identified as more than one race, and 2 did not know or did not report their race.

### 1.4.2 MRI acquisition and processing

Structural MRI scans for ABCD participants are collected using harmonized pulse sequences on one of seven possible MRI scanner models. The acquisition protocol included both a 3D MPRAGE T1- weighted volume (TE = 2-2.9ms, TR = 6.31 – 2500 ms, T1 = 1,060 ms, flip angle = 8 degrees, FOV = 256 x 256, resolution = 1 mm isotropic, slice thickness, slices = 176- 225) and a T2- weighted volume (TE = 60-565 ms, FOV = 256 x 256, resolution = 1mm isotropic, slices = 176-225). ABCD Twin hub participants used for this study were scanned using Siemans Prisma (N = 269), Siemans Prisma fit (N = 222) Philips Achieva dStream (N = 6), Phillips Ingenia (N = 102), and SIGNA Creator (N = 1). All structural MRI scans for HCP twin pairs were collected with a Siemens 3T Skyra scanner with a 32-channel head coil. The acquisition protocol included a 3D MPRAGE T1-weighted volume (TE = 2.14 ms, TR = 2,400 ms, TI = 1,000 ms, flip angle = 8 degrees, FOV = 224 x 224, in-plane resolution = 0.7 x 0.7 mm, slice thickness = 0.7 mm, slices = 256). The T1 and T2-weighted structural scans used for the child sample of this study were processed by the Developmental Cognition and Neuroimaging (DCAN) labs as part of the ABCD-BIDS Community Collection (ABCC). These methods are described in detail at the following webpage {(https://collection3165.readthedocs.io/en/stable/release_notes/)}. Subcortical segmentations for both HCP and ABCD Twin hub data were obtained by using automated segmentation tools to isolate subcortical structures (Fischl et al., 2002). Segmentation of hippocampal longitudinal and transverse-axis subregions was conducted using both T1 and T2

images from the Freesurfer v7.0 automated hippocampal subfield segmentation tool (Iglesias et al., 2015). This tool employs a probabilistic atlas built from a combination of 7T ultra-high field resolution, $0.13mm^3$, ex vivo, MRI scans, which were used to isolate hippocampal substructures, and a separate dataset of in vivo T1-weighted, $1mm^3$, MRI scans of the whole brain, which were used to isolate the total hippocampus from surrounding neural structures (e.g entorhinal cortex, amygdala).

### 1.4.3 Laterality Differences

Prior to conducting the primary analyses for this study, bivariate genetic models were used to determine the utility of aggregating hippocampal volume estimates across hemispheres. In line with previous work (Eyler et al., 2011; Elman et al., 2019), all regions of the hippocampus shared high degrees of genetic overlap across hemispheres for both the ABCD and HCP samples (i.e the confidence interval for the genetic correlation included 1; results shown in supplementary materials). This suggests there are little to no unique sources of genetic variance for the hippocampus of one hemisphere relative to the other. The heritability of hippocampal subregions and total volume was qualitatively lower for the left hemisphere relative to the right hemisphere, but with overlapping confidence intervals that indicated no statistically significant differences. Further, the results of all univariate and multivariate analyses did not differ across left and right hemispheres with respect to the primary hypotheses of this paper (see supplemental material for these analyses). As a result, hippocampal volume estimates were averaged across hemispheres for all primary analyses presented in this manuscript.

### 1.4.4 Univariate Modeling

Univariate biometric models were used to investigate the magnitude of genetic influence across hippocampal subregions. Biometric models attribute total phenotype variance to three

possible sources, primarily based on the differences in phenotypic correlation within MZ and DZ pairs. Additive genetic variance (denoted by A) represents the latent influence of segregating loci that are typically shared 100% and 50% identical-by-descent by members of MZ and DZ twin pairs respectively. Evidence for A arises when the MZ correlation is greater than the DZ correlation. Individual-specific environmental variance (denoted by E) includes person-specific factors and any influences of measurement error; E-associated variance is, in contrast to A, not shared between members of MZ or DZ twin pairs. Evidence for E arises from an MZ correlation than is statistically different from 1.0. While A and E are typically included as variance components in most biometric models, the third source of variance is selected based on the pattern of MZ and DZ twin pair correlations. Assuming that the influence of A as the sole source of twin similarity would result in a DZ correlation that is approximately half the magnitude of the MZ correlation, the third variance component is selected to be an additional, non-additive source of genetic similarity (denoted by D, for dominance genetics, or the interacting effects of loci) when the DZ correlation is considerably lower than half the MZ correlation. By contrast, a familial source of environmental variance (denoted by C, for twin-common environment) is modeled as the third variance component if, in contrast, the DZ correlation is considerably greater than half the MZ correlation. Once total variance has been attributed to one-to-three of these sources, narrow sense heritability is equal to $\frac{A}{A+C+E}$, or the proportion of total variance due to additive genetic variance (in the presence of D, broad and narrow sense heritability can also be estimated) (Neale and Cardon, 1992). In the results section of this manuscript, heritability refers to either narrow sense or broad sense heritability depending on the context. Subregions that are modeled as ADE are explicitly noted, and the heritability estimates of these regions represent broad sense heritability.

### 1.4.5 Multivariate Modeling

Multivariate models were used to investigate shared and unique sources of genetic variation across hippocampal subregions. Multivariate models build from the general univariate framework in order to decompose sources of covariation between phenotypes into shared sources of genetic and environmental variability. Although several parameterizations exist for multivariate genetic models (Verhulst, Prom-Wormley, Keller, Medland, and Neale, 2019), the following study utilized the Cholesky decomposition parameterization for all multivariate models. In cross-sectional study designs, the Cholesky decomposition represents shared sources of variance in a hierarchical fashion, where latent variables (factors) and their path coefficients are used to explain covariation across progressively smaller sets of variables within the model. The Cholesky decomposition is visually depicted in figure 1B. Although this parameterization yields latent variables for genetic and environmental effects, only the genetic effects are shown in these figures for expository purposes. The first genetic factor, represented as $A_1$ in figure 1B, prioritizes the first variable within the model; it explains the maximum amount of genetic variance in the first variable, while also capturing genetic variance in the second and third variables in the model. The second factor in the model explains the maximum amount of variance in the second variable that remains after accounting for the genetic effect of the first factor. As the first factor explained the maximum amount of genetic variance in the first variable, the second genetic factor does not include any sources of covariation with the first variable. The third and final factor explains the variance in the third variable that remains after accounting for the effects of the preceding two factors, and disregards shared genetic effects with the first and second variables within the model. Thus, the Cholesky parameterization represents sources of variance hierarchically in the sense that variables are ranked in terms of ordering within the model. As a result, the ordering of variables within the model will influence the value of the coefficients, although the ordering

of variables does not influence model fit (in most instances, including the present study). Cholesky decompositions were employed using three different variable orderings, in order to identify the unique genetic variance associated with the hippocampal head, body, and tail respectively. Unique genetic variance is represented by the third and final factor within the Cholesky model, and this factor represented different hippocampal subregions depending on their ordering within the model. In order to interpret the degree of genetic overlap between hippocampal subregions, path coefficients linking hippocampal subregions to one another were also converted to genetic correlations, which yield standardized measures of genetic covariation.

### 1.4.6 Model Selection

ACE models were employed for univariate analyses of all hippocampal subregions across both samples, except in cases where the ADE model provided a better fit relative to the ACE model (e.g ABCD Hippocampal tail, HCP hippocampal body and tail), in which case ADE models were used. For multivariate analyses, AE models were used in order to assess common and unique genetic influences across hippocampal subregions. These models provide greater interpretability given that several regions were better characterized by an ADE model rather than and ACE model. In addition, multivariate AE models provided a superior fit relative to ACE models in both samples (ABCD: $\vec{\Delta}$AIC = 11.80; p = 0.90; HCP: $\vec{\Delta}$AIC = 9.51; p = 0.87). The substantive conclusions of the results section do not depend on whether an AE or an ACE model was employed. Fit metrics for each of these models are displayed in the supplementary materials.

## 1.5 References


Neale, M. C., & Cardon, L. R. (1992). *Methodology for genetic studies of twins and families* [Pages: xxv, 496]. Kluwer Academic/Plenum Publishers. https://doi.org/10.1007/978-94-015-8018-2

Cardno, A. G., Marshall, E. J., Coid, B., Macdonald, A. M., Ribchester, T. R., Davies, N. J., Venturi, P., Jones, L. A., Lewis, S. W., Sham, P. C., Gottesman, I. I., Farmer, A. E., McGuffin, P., Reveley, A. M., & Murray, R. M. (1999). Heritability estimates for psychotic disorders: The maudsley twin psychosis series. *Archives of General Psychiatry*, *56*(2), 162–168. https://doi.org/10.1001/archpsyc.56.2.162

Maguire, E. A., Gadian, D. G., Johnsrude, I. S., Good, C. D., Ashburner, J., Frackowiak, R. S. J., & Frith, C. D. (2000). Navigation-related structural change in the hippocampi of taxi drivers [Publisher: Proceedings of the National Academy of Sciences]. *Proceedings of the National Academy of Sciences*, *97*(8), 4398–4403. https://doi.org/10.1073/pnas.070039597

Zhao, X., Lein, E. S., He, A., Smith, S. C., Aston, C., & Gage, F. H. (2001). Transcriptional profiling reveals strict boundaries between hippocampal subregions [_eprint: https://onlinelibrary.wiley.com/doi/pdf/10.1002/cne.1406]. *Journal of Comparative Neurology*, *441*(3), 187–196. https://doi.org/10.1002/cne.1406

Fischl, B., Salat, D. H., Busa, E., Albert, M., Dieterich, M., Haselgrove, C., van der Kouwe, A., Killiany, R., Kennedy, D., Klaveness, S., Montillo, A., Makris, N., Rosen, B., & Dale, A. M. (2002). Whole brain segmentation: Automated labeling of neuroanatomical structures in the human brain. *Neuron*, *33*(3), 341–355. https://doi.org/10.1016/S0896-6273(02)00569-X

Blakemore, S.-J., & Choudhury, S. (2006). Development of the adolescent brain: Implications for executive function and social cognition [_eprint: https://onlinelibrary.wiley.com/doi/pdf/10.1111/j.1469-7610.2006.01611.x]. *Journal of Child Psychology and Psychiatry*, *47*(3), 296–312. https://doi.org/10.1111/j.1469-7610.2006.01611.x

Maguire, E. A., Woollett, K., & Spiers, H. J. (2006). London taxi drivers and bus drivers: A structural MRI and neuropsychological analysis [_eprint: https://onlinelibrary.wiley.com/doi/pdf/10.1002/hipo.20233]. *Hippocampus*, *16*(12), 1091–1101. https://doi.org/10.1002/hipo.20233

Lisman, J. E., Coyle, J. T., Green, R. W., Javitt, D. C., Benes, F. M., Heckers, S., & Grace, A. A. (2008). Circuit-based framework for understanding neurotransmitter and risk gene interactions in schizophrenia. *Trends in Neurosciences*, *31*(5), 234–242. https://doi.org/10.1016/j.tins.2008.02.005

Thompson, C. L., Pathak, S. D., Jeromin, A., Ng, L. L., MacPherson, C. R., Mortrud, M. T., Cusick, A., Riley, Z. L., Sunkin, S. M., Bernard, A., Puchalski, R. B., Gage, F. H., Jones, A. R., Bajic, V. B., Hawrylycz, M. J., & Lein, E. S. (2008). Genomic anatomy of the hippocampus. *Neuron*, *60*(6), 1010–1021. https://doi.org/10.1016/j.neuron.2008.12.008

Fanselow, M. S., & Dong, H.-W. (2010). Are the dorsal and ventral hippocampus functionally distinct structures? *Neuron*, *65*(1), 7–19. https://doi.org/10.1016/j.neuron.2009.11.031

Insausti, R., Cebada-Sánchez, S., & Marcos, P. (2010). *Postnatal development of the human hippocampal formation* (Vol. 206). Springer Berlin Heidelberg. https://doi.org/10.1007/978-3-642-03661-3

Malykhin, N. V., Lebel, R. M., Coupland, N. J., Wilman, A. H., & Carter, R. (2010). In vivo quantification of hippocampal subfields using 4.7 t fast spin echo imaging. *NeuroImage*, *49*(2), 1224–1230. https://doi.org/10.1016/j.neuroimage.2009.09.042

Eyler, L. T., Prom-Wormley, E., Fennema-Notestine, C., Panizzon, M. S., Neale, M. C., Jernigan, T. L., Fischl, B., Franz, C. E., Lyons, M. J., Stevens, A., Pacheco, J., Perry,

M. E., Schmitt, J. E., Spitzer, N. C., Seidman, L. J., Thermenos, H. W., Tsuang, M. T., Dale, A. M., & Kremen, W. S. (2011). Genetic patterns of correlation among subcortical volumes in humans: Results from a magnetic resonance imaging twin study [_eprint: https://onlinelibrary.wiley.com/doi/pdf/10.1002/hbm.21054]. *Human Brain Mapping*, *32*(4), 641–653. https://doi.org/10.1002/hbm.21054

Lavenex, P., Sugden, S. G., Davis, R. R., Gregg, J. P., & Lavenex, P. B. (2011). Developmental regulation of gene expression and astrocytic processes may explain selective hippocampal vulnerability [_eprint: https://onlinelibrary.wiley.com/doi/pdf/10.1002/hipo.20730]. *Hippocampus*, *21*(2), 142–149. https://doi.org/10.1002/hipo.20730

McEwen, B. S. (2012). Brain on stress: How the social environment gets under the skin [Publisher: Proceedings of the National Academy of Sciences]. *Proceedings of the National Academy of Sciences*, *109*, 17180–17185. https://doi.org/10.1073/pnas.1121254109

Beam, C. R., & Turkheimer, E. (2013). Phenotype-environment correlations in longitudinal twin models. *Development and Psychopathology*, *25*(1), 7–16. https://doi.org/10.1017/S0954579412000867

Bouchard, T. J. (2013). The wilson effect: The increase in heritability of IQ with age [Publisher: Cambridge University Press]. *Twin Research and Human Genetics*, *16*(5), 923–930. https://doi.org/10.1017/thg.2013.54

Lavenex, P., & Banta Lavenex, P. (2013). Building hippocampal circuits to learn and remember: Insights into the development of human memory. *Behavioural Brain Research*, *254*, 8–21. https://doi.org/10.1016/j.bbr.2013.02.007

Poppenk, J., Evensmoen, H. R., Moscovitch, M., & Nadel, L. (2013). Long-axis specialization of the human hippocampus. *Trends in Cognitive Sciences*, *17*(5), 230–240. https://doi.org/10.1016/j.tics.2013.03.005

Van Essen, D. C., Smith, S. M., Barch, D. M., Behrens, T. E. J., Yacoub, E., Ugurbil, K., & WU-Minn HCP Consortium. (2013). The WU-minn human connectome project: An overview. *NeuroImage*, *80*, 62–79. https://doi.org/10.1016/j.neuroimage.2013.05.041

Batouli, S. A. H., Trollor, J. N., Wen, W., & Sachdev, P. S. (2014). The heritability of volumes of brain structures and its relationship to age: A review of twin and family studies. *Ageing Research Reviews*, *13*, 1–9. https://doi.org/10.1016/j.arr.2013.10.003

Pipitone, J., Park, M. T. M., Winterburn, J., Lett, T. A., Lerch, J. P., Pruessner, J. C., Lepage, M., Voineskos, A. N., & Chakravarty, M. M. (2014). Multi-atlas segmentation of the whole hippocampus and subfields using multiple automatically generated templates. *NeuroImage*, *101*, 494–512. https://doi.org/10.1016/j.neuroimage.2014.04.054

Strange, B. A., Witter, M. P., Lein, E. S., & Moser, E. I. (2014). Functional organization of the hippocampal longitudinal axis [Bandiera_abtest: a Cg_type: Nature Research Journals Number: 10 Primary_atype: Reviews Publisher: Nature Publishing Group Subject_term: Hippocampus Subject_term_id: hippocampus]. *Nature Reviews Neuroscience*, *15*(10), 655–669. https://doi.org/10.1038/nrn3785

Swagerman, S. C., Brouwer, R. M., de Geus, E. J. C., Hulshoff Pol, H. E., & Boomsma, D. I. (2014). Development and heritability of subcortical brain volumes at ages 9 and 12 [_eprint: https://onlinelibrary.wiley.com/doi/pdf/10.1111/gbb.12182]. *Genes, Brain and Behavior*, *13*(8), 733–742. https://doi.org/10.1111/gbb.12182

Wisse, L. E. M., Biessels, G. J., & Geerlings, M. I. (2014). A critical appraisal of the hippocampal subfield segmentation package in FreeSurfer. *Frontiers in Aging Neuroscience*, *6*, 261. https://doi.org/10.3389/fnagi.2014.00261

Iglesias, J. E., Augustinack, J. C., Nguyen, K., Player, C. M., Player, A., Wright, M., Roy, N., Frosch, M. P., McKee, A. C., Wald, L. L., Fischl, B., & Van Leemput, K. (2015). A computational atlas of the hippocampal formation using ex vivo, ultra-high resolution

MRI: Application to adaptive segmentation of in vivo MRI. *NeuroImage*, *115*, 117–137. https://doi.org/10.1016/j.neuroimage.2015.04.042

Yushkevich, P. A., Pluta, J. B., Wang, H., Xie, L., Ding, S.-L., Gertje, E. C., Mancuso, L., Kliot, D., Das, S. R., & Wolk, D. A. (2015). Automated volumetry and regional thickness analysis of hippocampal subfields and medial temporal cortical structures in mild cognitive impairment [_eprint: https://onlinelibrary.wiley.com/doi/pdf/10.1002/hbm.22627]. *Human Brain Mapping*, *36*(1), 258–287. https://doi.org/10.1002/hbm.22627

Briley, D. A., & Tucker-Drob, E. M. (2017). Comparing the developmental genetics of cognition and personality over the lifespan. *Journal of personality*, *85*(1), 51–64. https://doi.org/10.1111/jopy.12186

Patel, S., Park, M. T. M., Devenyi, G. A., Patel, R., Masellis, M., Knight, J., & Chakravarty, M. M. (2017). Heritability of hippocampal subfield volumes using a twin and non-twin siblings design [_eprint: https://onlinelibrary.wiley.com/doi/pdf/10.1002/hbm.23654]. *Human Brain Mapping*, *38*(9), 4337–4352. https://doi.org/10.1002/hbm.23654

Iacono, W. G., Heath, A. C., Hewitt, J. K., Neale, M. C., Banich, M. T., Luciana, M. M., Madden, P. A., Barch, D. M., & Bjork, J. M. (2018). The utility of twins in developmental cognitive neuroscience research: How twins strengthen the ABCD research design. *Developmental Cognitive Neuroscience*, *32*, 30–42. https://doi.org/10.1016/j.dcn.2017.09.001

McHugo, M., Talati, P., Woodward, N. D., Armstrong, K., Blackford, J. U., & Heckers, S. (2018). Regionally specific volume deficits along the hippocampal long axis in early and chronic psychosis. *NeuroImage: Clinical*, *20*, 1106–1114. https://doi.org/10.1016/j.nicl.2018.10.021

Elman, J. A., Panizzon, M. S., Gillespie, N. A., Hagler Jr., D. J., Fennema-Notestine, C., Eyler, L. T., McEvoy, L. K., Neale, M. C., Lyons, M. J., Franz, C. E., Dale, A. M., & Kremen, W. S. (2019). Genetic architecture of hippocampal subfields on

standard resolution MRI: How the parts relate to the whole [_eprint: https://onlinelibrary.wiley.com/doi/pdf/10.1002/hbm.24464]. *Human Brain Mapping*, *40*(5), 1528–1540. https://doi.org/10.1002/hbm.24464

Langnes, E., Vidal-Piñeiro, D., Sneve, M. H., Amlien, I. K., Walhovd, K. B., & Fjell, A. M. (2019). Development and decline of the hippocampal long-axis specialization and differentiation during encoding and retrieval of episodic memories. *Cerebral Cortex*, *29*(8), 3398–3414. https://doi.org/10.1093/cercor/bhy209

Verhulst, B., Prom-Wormley, E., Keller, M., Medland, S., & Neale, M. C. (2019). Type i error rates and parameter bias in multivariate behavioral genetic models. *Behavior Genetics*, *49*(1), 99–111. https://doi.org/10.1007/s10519-018-9942-y

Langnes, E., Sneve, M. H., Sederevicius, D., Amlien, I. K., Walhovd, K. B., & Fjell, A. M. (2020). Anterior and posterior hippocampus macro- and microstructure across the lifespan in relation to memory—a longitudinal study [_eprint: https://onlinelibrary.wiley.com/doi/pdf/10.1002/hipo.23189]. *Hippocampus*, *30*(7), 678–692. https://doi.org/10.1002/hipo.23189

McHugo, M., Armstrong, K., Roeske, M. J., Woodward, N. D., Blackford, J. U., & Heckers, S. (2020). Hippocampal volume in early psychosis: A 2-year longitudinal study [Number: 1 Publisher: Nature Publishing Group]. *Translational Psychiatry*, *10*(1), 1–10. https://doi.org/10.1038/s41398-020-00985-1

van der Meer, D., Rokicki, J., Kaufmann, T., Córdova-Palomera, A., Moberget, T., Alnæs, D., Bettella, F., Frei, O., Doan, N. T., Sønderby, I. E., Smeland, O. B., Agartz, I., Bertolino, A., Bralten, J., Brandt, C. L., Buitelaar, J. K., Djurovic, S., van Donkelaar, M., Dørum, E. S., … Pediatric Imaging, Neurocognition and Genetics Study. (2020). Brain scans from 21,297 individuals reveal the genetic architecture of hippocampal subfield volumes. *Molecular Psychiatry*, *25*(11), 3053–3065. https://doi.org/10.1038/s41380-018-0262-7

Vogel, J. W., La Joie, R., Grothe, M. J., Diaz-Papkovich, A., Doyle, A., Vachon-Presseau, E., Lepage, C., Vos de Wael, R., Thomas, R. A., Iturria-Medina, Y., Bernhardt, B., Rabinovici, G. D., & Evans, A. C. (2020). A molecular gradient along the longitudinal axis of the human hippocampus informs large-scale behavioral systems [Bandiera_abtest: a Cc_license_type: cc_by Cg_type: Nature Research Journals Number: 1 Primary_atype: Research Publisher: Nature Publishing Group Subject_term: Cognitive neuroscience;Genetics of the nervous system;Molecular neuroscience Subject_term_id: cognitive-neuroscience;genetics-of-the-nervous-system;molecular-neuroscience]. *Nature Communications*, *11*(1), 960. https://doi.org/10.1038/s41467-020-14518-3

Bahrami, S., Nordengen, K., Shadrin, A. A., Frei, O., Meer, D. v. d., Dale, A. M., Westlye, L. T., Andreassen, O. A., & Kaufmann, T. (2021, August 24). *Distributed genetic architecture across the hippocampal formation implies common neuropathology across major brain disorders* [Company: Cold Spring Harbor Laboratory Press Distributor: Cold Spring Harbor Laboratory Press Label: Cold Spring Harbor Laboratory Press Type: article]. https://doi.org/10.1101/2021.08.18.21262223

Bayrak, S., Vos de Wael, R., Schaare, H. L., Caldairou, B., Bernasconi, A., Bernasconi, N., Bernhardt, B. C., & Valk, S. L. (2021, November 11). *Heritability of hippocampal functional and microstructural organisation* (preprint). Neuroscience. https://doi.org/10.1101/2021.11.10.468049

Conley, M. I., Skalaban, L. J., Rapuano, K. M., Gonzalez, R., Laird, A. R., Dick, A. S., Sutherland, M. T., Watts, R., & Casey, B. (2021). Altered hippocampal microstructure and function in children who experienced hurricane irma [_eprint: https://onlinelibrary.wiley.com/doi/pdf/10.1002/dev.22071]. *Developmental Psychobiology*, *63*(5), 864–877. https://doi.org/10.1002/dev.22071

Kahhale, I., Buser, N. J., Madan, C. R., & Hanson, J. L. (2021, October 29). *Quantifying numerical and spatial reliability of amygdala and hippocampal subdivisions in FreeSurfer*

[Company: Cold Spring Harbor Laboratory Distributor: Cold Spring Harbor Laboratory Label: Cold Spring Harbor Laboratory Section: New Results Type: article]. https://doi.org/10.1101/2020.06.12.149203

Le Grand, Q., Satizabal, C. L., Sargurupremraj, M., Mishra, A., Soumaré, A., Laurent, A., Crivello, F., Tsuchida, A., Shin, J., Macalli, M., Singh, B., Beiser, A. S., DeCarli, C., Fletcher, E., Paus, T., Lathrop, M., Adams, H. H., Bis, J. C., Seshadri, S., … Debette, S. (2021). Genomic studies across the lifespan point to early mechanisms determining subcortical volumes. *Biological Psychiatry: Cognitive Neuroscience and Neuroimaging*, S245190222100286X. https://doi.org/10.1016/j.bpsc.2021.10.011

Plassard, A. J., Bao, S., McHugo, M., Beason-Held, L., Blackford, J. U., Heckers, S., & Landman, B. A. (2021). Automated, open-source segmentation of the hippocampus and amygdala with the open vanderbilt archive of the temporal lobe. *Magnetic Resonance Imaging*, *81*, 17–23. https://doi.org/10.1016/j.mri.2021.04.011

Sahakyan, L., Meller, T., Evermann, U., Schmitt, S., Pfarr, J.-K., Sommer, J., Kwapil, T. R., & Nenadić, I. (2021). Anterior vs posterior hippocampal subfields in an extended psychosis phenotype of multidimensional schizotypy in a nonclinical sample. *Schizophrenia Bulletin*, *47*(1), 207–218. https://doi.org/10.1093/schbul/sbaa099

Seiger, R., Hammerle, F. P., Godbersen, G. M., Reed, M. B., Spurny-Dworak, B., Handschuh, P., Klöbl, M., Unterholzner, J., Gryglewski, G., Vanicek, T., & Lanzenberger, R. (2021). Comparison and reliability of hippocampal subfield segmentations within FreeSurfer utilizing t1- and t2-weighted multispectral MRI data. *Frontiers in Neuroscience*, *15*, 666000. https://doi.org/10.3389/fnins.2021.666000

Wisse, L. E. M., Chételat, G., Daugherty, A. M., de Flores, R., la Joie, R., Mueller, S. G., Stark, C. E. L., Wang, L., Yushkevich, P. A., Berron, D., Raz, N., Bakker, A., Olsen, R. K., & Carr, V. A. (2021). Hippocampal subfield volumetry from structural

isotropic 1 mm3 MRI scans: A note of caution [_eprint: https://onlinelibrary.wiley.com/doi/pdf/10.1002/hbm.25234]. *Human Brain Mapping*, *42*(2), 539–550. https://doi.org/10.1002/hbm.25234

# Chapter 2

# Supplementary Materials

## 2.1 Supplementary Table 1

Supplementary Table 2.1: Model fit metrics for longitudinal axis subregions in ABCD subjects

| Brain Region | | | Head | | | Body | | | Tail | | | Whole | | |
|---|---|---|---|---|---|---|---|---|---|---|---|---|---|---|
| | Model | df | rank | AIC | p | rank | AIC | p | rank | AIC | p | rank | AIC | p |
| Left Hippocampus | ACE | 1422 | 1 | 3415 | 0.91 | 2 | 3708 | 0.78 | 3 | 3649.50 | 0.41 | 1 | 3449.43 | 0.94 |
| | ADE | 1422 | 3 | 3421 | 0.29 | 3 | 3709 | 0.73 | 1 | 3645.20 | 0.94 | 3 | 3451.83 | 0.65 |
| | AE | 1423 | 2 | 3419 | 0.4 | 1 | 3707 | 0.82 | 2 | 3647.50 | 0.53 | 2 | 3449.83 | 0.75 |
| | CE | 1423 | 4 | 3496 | >0.01 | 4 | 3740 | >0.01 | 4 | 3739.49 | >0.01 | 4 | 3524.68 | >0.01 |
| | E | 1424 | 5 | 3849 | >0.01 | 5 | 3918 | >0.01 | 5 | 3925.92 | >0.01 | 5 | 3837.62 | >0.01 |
| Right Hippocampus | ACE | 1422 | 2 | 3410 | 0.79 | 2 | 3484 | 0.99 | 3 | 3690.54 | 0.88 | 2 | 3325.40 | 0.94 |
| | ADE | 1422 | 2 | 3410 | 0.78 | 3 | 3485 | 0.98 | 2 | 3689.83 | 0.95 | 3 | 3325.41 | 0.94 |
| | AE | 1423 | 1 | 3408 | 0.87 | 1 | 3483 | 0.99 | 1 | 3688.54 | 0.94 | 1 | 3323.41 | 0.97 |
| | CE | 1423 | 4 | 3532 | >0.01 | 4 | 3575 | >0.01 | 4 | 3752.97 | >0.01 | 4 | 3475.16 | >0.01 |
| | E | 1424 | 5 | 3837 | >0.01 | 5 | 3868 | >0.01 | 5 | 3941.78 | >0.01 | 5 | 3810.32 | >0.01 |
| Averaged Hippocampus | ACE | 1422 | 1 | 3269 | 0.87 | 2 | 3477 | 0.96 | 3 | 3558.45 | 0.71 | 2 | 3249.20 | 0.94 |
| | ADE | 1422 | 3 | 3272 | 0.56 | 3 | 3478 | 0.95 | 1 | 3556.18 | 0.96 | 3 | 3250.20 | 0.83 |
| | AE | 1423 | 2 | 3270 | 0.68 | 1 | 3476 | 0.98 | 2 | 3556.45 | 0.81 | 1 | 3248.20 | 0.9 |
| | CE | 1423 | 4 | 3424 | >0.01 | 4 | 3578 | >0.01 | 4 | 3676.27 | >0.01 | 4 | 3417.09 | >0.01 |
| | E | 1424 | 5 | 3825 | >0.01 | 5 | 3873 | >0.01 | 5 | 3917.84 | >0.01 | 5 | 3806.72 | >0.01 |

## 2.2 Supplementary Table 2

Supplementary Table 2.2: Model fit metrics for longitudinal axis subregions in HCP subjects

| Brain Region | | | Head | | | Body | | | Tail | | | Whole | | |
|---|---|---|---|---|---|---|---|---|---|---|---|---|---|---|
| | Model | df | rank | AIC | p | rank | AIC | p | rank | AIC | p | rank | AIC | p |
| Left Hippocampus | ACE | 430 | 2 | 921 | 0.37 | 3 | 1032 | 0.26 | 3 | 1073.30 | 0.74 | 2 | 909.86 | 0.82 |
| | ADE | 430 | 2 | 921 | 0.37 | 2 | 1031 | 0.26 | 2 | 1073.12 | 0.76 | 2 | 909.86 | 0.82 |
| | AE | 431 | 1 | 920 | 0.46 | 1 | 1030 | 0.36 | 1 | 1071.30 | 0.83 | 1 | 907.89 | 0.89 |
| | CE | 431 | 4 | 966 | >0.01 | 4 | 1053 | >0.01 | 4 | 1103.84 | >0.01 | 4 | 962.62 | >0.01 |
| | E | 432 | 5 | 1121 | >0.01 | 5 | 1152 | >0.01 | 5 | 1203.78 | >0.01 | 5 | 1120.38 | >0.01 |
| Right Hippocampus | ACE | 430 | 3 | 931 | 0.57 | 3 | 936 | 0.74 | 3 | 1070.61 | 0.28 | 3 | 878.83 | 0.78 |
| | ADE | 430 | 2 | 931 | 0.57 | 2 | 935 | 0.87 | 2 | 1070.23 | 0.32 | 2 | 878.54 | 0.81 |
| | AE | 431 | 1 | 929 | 0.69 | 1 | 934 | 0.83 | 1 | 1068.61 | 0.39 | 1 | 876.83 | 0.86 |
| | CE | 431 | 4 | 987 | >0.01 | 4 | 998 | >0.01 | 4 | 1101.58 | >0.01 | 4 | 961.17 | >0.01 |
| | E | 432 | 5 | 1133 | >0.01 | 5 | 1130 | >0.01 | 5 | 1192.88 | >0.01 | 5 | 1117.87 | >0.01 |
| Average Hippocampus | ACE | 430 | 2 | 863 | 0.42 | 3 | 935 | 0.85 | 3 | 1031.23 | 0.42 | 2 | 834.19 | 0.79 |
| | ADE | 430 | 2 | 863 | 0.42 | 2 | 935 | 0.88 | 2 | 1031.16 | 0.43 | 2 | 834.19 | 0.79 |
| | AE | 431 | 1 | 861 | 0.53 | 1 | 933 | 0.91 | 1 | 1029.23 | 0.54 | 1 | 832.19 | 0.87 |
| | CE | 431 | 4 | 942 | >0.01 | 4 | 992 | >0.01 | 4 | 1074.03 | >0.01 | 4 | 930.43 | >0.01 |
| | E | 432 | 5 | 1121 | >0.01 | 5 | 1133 | >0.01 | 5 | 1195.00 | >0.01 | 5 | 1113.18 | >0.01 |

## 2.3 Supplementary Table 3

Supplementary Table 2.3: Model output for longitudinal axis subregions for right hemisphere in both ABCD and HCP subjects

| Sample | Subregion | $DZ_r$ | $MZ_r$ | Heritability ($h^2$) | Common Environment ($c$) | Unique Environment ($e$) |
|---|---|---|---|---|---|---|
| ABCD | Right Head | 0.82 | 0.42 | 0.82 (0.67-0.86) | 0.00 (0.00-0.15) | 0.17 (0.14-0.21) |
| | Right Body | 0.80 | 0.42 | 0.75 (0.60-0.83) | 0.04 (0.00-0.19) | 0.21 (0.17-0.24) |
| | Right Tail* | 0.70 | 0.32 | 0.71 (0.65-0.75) | NA (NA-NA) | 0.29 (0.25-0.35) |
| | Right Whole* | 0.85 | 0.43 | 0.85 (0.70-0.88) | 0.01 (0.00-0.15) | 0.14 (0.12-0.17) |
| HCP | Right Head* | 0.86 | 0.43 | 0.87 (0.82-0.90) | NA (NA-NA) | 0.13 (0.10-0.18) |
| | Right Body* | 0.87 | 0.32 | 0.86 (0.81-0.89) | NA (NA-NA) | 0.14 (0.11-0.19) |
| | Right Tail* | 0.76 | 0.36 | 0.77 (0.70-0.83) | NA (NA-NA) | 0.23 (0.17-0.30) |
| | Right Whole* | 0.90 | 0.40 | 0.90 (0.87-0.92) | NA (NA-NA) | 0.10 (0.08-0.13) |

*Note*: Asterisk (*) indicates ADE model used instead of ACE.

## 2.4 Supplementary Table 4

Supplementary Table 2.4: Model output for longitudinal axis subregions for left hemisphere in both ABCD and HCP subjects

| Sample | Subregion | $DZ_r$ | $MZ_r$ | Heritability ($h^2$) | Common Environment ($c$) | Unique Environment ($e$) |
|---|---|---|---|---|---|---|
| ABCD | Left Head | 0.80 | 0.50 | 0.64 (0.50-0.79) | 0.17 (0.03-0.30) | 0.19 (0.16-0.22) |
| | Left Body | 0.64 | 0.35 | 0.59 (0.39-0.70) | 0.06 (0.00-0.22) | 0.36 (0.30-0.42) |
| | Left Tail* | 0.74 | 0.29 | 0.75 (0.70-0.79) | NA (NA-NA) | 0.25 (0.21-0.30) |
| | Left Whole | 0.78 | 0.46 | 0.67 (0.52-0.81) | 0.12 (0.00-0.26) | 0.21 (0.18-0.25) |
| HCP | left head | 0.86 | 0.45 | 0.79 (0.50-0.89) | 0.07 (0.00-0.36) | 0.14 (0.11-0.19) |
| | left body* | 0.75 | 0.38 | 0.75 (0.67-0.81) | NA (NA-NA) | 0.25 (0.19-0.33) |
| | left tail* | 0.77 | 0.37 | 0.78 (0.71-0.83) | NA (NA-NA) | 0.22 (0.17-0.29) |
| | left whole | 0.87 | 0.43 | 0.84 (0.54-0.90) | 0.03 (0.00-0.32) | 0.13 (0.10-0.17) |

*Note*: Asterisk (*) indicates ADE model used instead of ACE.

## 2.5 Supplementary Table 5

Supplementary Table 2.5: Genetic correlations between long-axis subregions of the left and right hemispheres, using ACE model parameterization

| Sample | Hippocampal Subregion | Genetic Correlation |
|---|---|---|
| ABCD | Head | 0.98 (0.91-1.00) |
| | Body | 1.00 (0.88-1.00) |
| | Tail | 0.93 (0.83-1.00) |
| | Whole | 1.00 (0.93-1.00) |
| HCP | Head | 0.91 (0.81-1.00) |
| | Body | 1.00 (0.90-1.00) |
| | Tail | 0.86 (0.71-0.99) |
| | Whole | 0.96 (0.88-1.00) |

## 2.6 Supplementary Table 6

Supplementary Table 2.6: Genetic correlations between long-axis subregions of the left and right hemispheres, using AE model parameterization

| Sample | Hippocampal Subregion | Genetic Correlation |
|---|---|---|
| ABCD | Head | 0.97 (0.95-1.00) |
| | Body | 0.93 (0.90-0.97) |
| | Tail | 0.93 (0.89-0.97) |
| | Whole | 0.98 (0.96-1.00) |
| HCP | Head | 0.98 (0.96-1.00) |
| | Body | 0.96 (0.91-1.00) |
| | Tail | 0.96 (0.91-1.00) |
| | Whole | 0.98 (0.96-1.00) |

## 2.7 Supplementary Table 7

Supplementary Table 2.7: Output from Trivariate Cholesky Model using ACE parameterization

| | Factor | Factor Loading | ABCD | HCP |
|---|---|---|---|---|
| Hippocampal Head as A3 | A1: Tail | a11: Tail | 0.78 (0.69-0.82) | 0.76 (0.54-0.86) |
| | A1: Tail | a21: Body | 0.33 (0.24-0.42) | 0.51 (0.29-0.70) |
| | A1: Tail | a31: Head | 0.16 (0.10-0.24) | 0.13 (0.03-0.28) |
| | A2: Body | a12: Tail | NA (NA-NA) | NA (NA-NA) |
| | A2: Body | a22: Body | 0.42 (0.31-0.49) | 0.32 (0.12-0.50) |
| | A2: Body | a32: Head | 0.32 (0.22-0.44) | 0.45 (0.19-0.78) |
| | A3: Head | a31: Tail | NA (NA-NA) | NA (NA-NA) |
| | A3: Head | a32: Body | NA (NA-NA) | NA (NA-NA) |
| | A3: Head | a33: Head | 0.28 (0.20-0.34) | 0.28 (NA-0.44) |
| Hippocampal Body as A3 | A1: Head | a11: Head | 0.76 (0.63-0.89) | 0.86 (0.59-0.93) |
| | A1: Head | a21: Tail | 0.17 (0.10-0.24) | 0.11 (0.02-0.25) |
| | A1: Head | a31: Body | 0.47 (0.35-0.58) | 0.47 (0.27-0.61) |
| | A2: Tail | a12: Head | NA (NA-NA) | NA (NA-NA) |
| | A2: Tail | a22: Tail | 0.61 (0.54-0.66) | 0.65 (0.43-0.77) |
| | A2: Tail | a32: Body | 0.09 (0.05-0.13) | 0.24 (0.12-0.37) |
| | A3: Body | a31: Head | NA (NA-NA) | NA (NA-NA) |
| | A3: Body | a32: Tail | NA (NA-NA) | NA (NA-NA) |
| | A3: Body | a33: Body | 0.19 (0.12-0.23) | 0.12 (NA-0.24) |
| Hippocampal Tail as A3 | A1: Head | a11: Head | 0.76 (0.63-0.89) | 0.86 (0.59-0.93) |
| | A1: Head | a21: Body | 0.47 (0.35-0.58) | 0.47 (0.27-0.61) |
| | A1: Head | a31: Tail | 0.17 (0.10-0.24) | 0.11 (0.02-0.25) |
| | A2: Body | a12: Head | NA (NA-NA) | NA (NA-NA) |
| | A2: Body | a22: Body | 0.28 (0.20-0.33) | 0.36 (0.22-0.46) |
| | A2: Body | a32: Tail | 0.19 (0.13-0.28) | 0.43 (0.22-0.67) |
| | A3: Tail | a31: Head | NA (NA-NA) | NA (NA-NA) |
| | A3: Tail | a32: Body | NA (NA-NA) | NA (NA-NA) |
| | A3: Tail | a33: Tail | 0.42 (0.33-0.48) | 0.22 (NA-0.43) |

## 2.8 Supplementary Table 8

Supplementary Table 2.8: Output from Trivariate Cholesky Model for left hemishpere using ACE parameterization

| | Factor | Factor Loading | ABCD | HCP |
|---|---|---|---|---|
| Hippocampal Left Head as A3 | A1: Left Tail | a11: Left Tail | 0.70 (0.61-0.76) | 0.74 (0.49-0.83) |
| | A1: Left Tail | a21: Left Body | 0.24 (0.15-0.34) | 0.43 (0.20-0.66) |
| | A1: Left Tail | a31: Left Head | 0.12 (0.06-0.20) | 0.17 (0.04-0.35) |
| | A2: Left Body | a12: Left Tail | NA (NA-NA) | NA (NA-NA) |
| | A2: Left Body | a22: Left Body | 0.31 (0.17-0.41) | 0.20 (0.01-0.45) |
| | A2: Left Body | a32: Left Head | 0.28 (0.15-0.44) | 0.29 (0.03-0.76) |
| | A3: Left Head | a31: Left Tail | NA (NA-NA) | NA (NA-NA) |
| | A3: Left Head | a32: Left Body | NA (NA-NA) | NA (NA-NA) |
| | A3: Left Head | a33: Left Head | 0.24 (0.13-0.33) | 0.31 (NA-0.46) |
| Hippocampal Left Body as A3 | A1: Left Head | a11: Left Head | 0.64 (0.50-0.79) | 0.77 (0.49-0.89) |
| | A1: Left Head | a21: Left Tail | 0.14 (0.07-0.22) | 0.16 (0.04-0.33) |
| | A1: Left Head | a31: Left Body | 0.34 (0.20-0.49) | 0.34 (0.15-0.55) |
| | A2: Left Tail | a12: Left Head | NA (NA-NA) | NA (NA-NA) |
| | A2: Left Tail | a22: Left Tail | 0.57 (0.50-0.62) | 0.58 (0.34-0.71) |
| | A2: Left Tail | a32: Left Body | 0.07 (0.03-0.11) | 0.19 (0.06-0.34) |
| | A3: Left Body | a31: Left Head | NA (NA-NA) | NA (NA-NA) |
| | A3: Left Body | a32: Left Tail | NA (NA-NA) | NA (NA-NA) |
| | A3: Left Body | a33: Left Body | 0.14 (0.04-0.21) | 0.10 (0.00-0.25) |
| Hippocampal Left Tail as A3 | A1: Left Head | a11: Left Head | 0.64 (0.50-0.79) | 0.77 (0.49-0.89) |
| | A1: Left Head | a21: Left Body | 0.34 (0.20-0.49) | 0.34 (0.15-0.55) |
| | A1: Left Head | a31: Left Tail | 0.14 (0.07-0.22) | 0.16 (0.04-0.33) |
| | A2: Left Body | a12: Left Head | NA (NA-NA) | NA (NA-NA) |
| | A2: Left Body | a22: Left Body | 0.21 (0.10-0.29) | 0.29 (0.10-0.41) |
| | A2: Left Body | a32: Left Tail | 0.19 (0.10-0.32) | 0.37 (0.12-0.69) |
| | A3: Left Tail | a31: Left Head | NA (NA-NA) | NA (NA-NA) |
| | A3: Left Tail | a32: Left Body | NA (NA-NA) | NA (NA-NA) |
| | A3: Left Tail | a33: Left Tail | 0.38 (0.20-0.46) | 0.21 (0.00-0.46) |

## 2.9 Supplementary Table 9

Supplementary Table 2.9: Output from Trivariate Cholesky Model for right hemishpere using ACE parameterization

| | Factor | Factor Loading | ABCD | HCP |
|---|---|---|---|---|
| Hippocampal Right Head as A3 | A1: Right Tail | a11: Right Tail | 0.70 (0.57-0.75) | 0.76 (0.51-0.82) |
| | A1: Right Tail | a21: Right Body | 0.36 (0.24-0.49) | 0.40 (0.22-0.53) |
| | A1: Right Tail | a31: Right Head | 0.17 (0.10-0.25) | 0.10 (0.02-0.24) |
| | A2: Right Body | a12: Right Tail | NA (NA-NA) | NA (NA-NA) |
| | A2: Right Body | a22: Right Body | 0.38 (0.24-0.50) | 0.45 (0.32-0.56) |
| | A2: Right Body | a32: Right Head | 0.36 (0.22-0.49) | 0.48 (0.27-0.71) |
| | A3: Right Head | a31: Right Tail | NA (NA-NA) | NA (NA-NA) |
| | A3: Right Head | a32: Right Body | NA (NA-NA) | NA (NA-NA) |
| | A3: Right Head | a33: Right Head | 0.29 (0.21-0.35) | 0.18 (NA-0.39) |
| Hippocampal Right Body as A3 | A1: Right Head | a11: Right Head | 0.82 (0.67-0.85) | 0.76 (0.54-0.89) |
| | A1: Right Head | a21: Right Tail | 0.15 (0.09-0.21) | 0.10 (0.02-0.23) |
| | A1: Right Head | a31: Right Body | 0.47 (0.35-0.57) | 0.58 (0.37-0.76) |
| | A2: Right Tail | a12: Right Head | NA (NA-NA) | NA (NA-NA) |
| | A2: Right Tail | a22: Right Tail | 0.55 (0.44-0.61) | 0.66 (0.45-0.75) |
| | A2: Right Tail | a32: Right Body | 0.10 (0.05-0.17) | 0.14 (0.03-0.28) |
| | A3: Right Body | a31: Right Head | NA (NA-NA) | NA (NA-NA) |
| | A3: Right Body | a32: Right Tail | NA (NA-NA) | NA (NA-NA) |
| | A3: Right Body | a33: Right Body | 0.17 (0.08-0.24) | 0.13 (0.00-0.24) |
| Hippocampal Right Tail as A3 | A1: Right Head | a11: Right Head | 0.82 (0.67-0.85) | 0.76 (0.54-0.89) |
| | A1: Right Head | a21: Right Body | 0.47 (0.35-0.57) | 0.58 (0.37-0.77) |
| | A1: Right Head | a31: Right Tail | 0.15 (0.09-0.21) | 0.10 (0.02-0.23) |
| | A2: Right Body | a12: Right Head | NA (NA-NA) | NA (NA-NA) |
| | A2: Right Body | a22: Right Body | 0.27 (0.18-0.34) | 0.27 (0.07-0.43) |
| | A2: Right Body | a32: Right Tail | 0.21 (0.11-0.35) | 0.35 (0.10-0.71) |
| | A3: Right Tail | a31: Right Head | NA (NA-NA) | NA (NA-NA) |
| | A3: Right Tail | a32: Right Body | NA (NA-NA) | NA (NA-NA) |
| | A3: Right Tail | a33: Right Tail | 0.35 (0.19-0.44) | 0.31 (0.00-0.44) |

## 2.10 Supplementary Table 10

Supplementary Table 2.10: Output from Trivariate Cholesky Model using AE parameterization

| | Factor | Factor Loading | ABCD | HCP |
|---|---|---|---|---|
| Hippocampal Head as A3 | A1: Tail | a11: Tail | 0.80 (0.76-0.83) | 0.83 (0.77-0.87) |
| | A1: Tail | a21: Body | 0.36 (0.31-0.42) | 0.43 (0.34-0.53) |
| | A1: Tail | a31: Head | 0.20 (0.15-0.25) | 0.13 (0.06-0.22) |
| | A2: Body | a12: Tail | NA (NA-NA) | NA (NA-NA) |
| | A2: Body | a22: Body | 0.44 (0.39-0.49) | 0.43 (0.34-0.52) |
| | A2: Body | a32: Head | 0.36 (0.31-0.42) | 0.41 (0.31-0.52) |
| | A3: Head | a31: Tail | NA (NA-NA) | NA (NA-NA) |
| | A3: Head | a32: Body | NA (NA-NA) | NA (NA-NA) |
| | A3: Head | a33: Head | 0.31 (0.27-0.35) | 0.37 (0.29-0.46) |
| Hippocampal Body as A3 | A1: Head | a11: Head | 0.88 (0.85-0.90) | 0.91 (0.88-0.93) |
| | A1: Head | a21: Tail | 0.18 (0.14-0.23) | 0.12 (0.05-0.20) |
| | A1: Head | a31: Body | 0.51 (0.47-0.56) | 0.47 (0.38-0.56) |
| | A2: Tail | a12: Head | NA (NA-NA) | NA (NA-NA) |
| | A2: Tail | a22: Tail | 0.61 (0.56-0.67) | 0.71 (0.63-0.79) |
| | A2: Tail | a32: Body | 0.09 (0.06-0.12) | 0.19 (0.12-0.26) |
| | A3: Body | a31: Head | NA (NA-NA) | NA (NA-NA) |
| | A3: Body | a32: Tail | NA (NA-NA) | NA (NA-NA) |
| | A3: Body | a33: Body | 0.20 (0.17-0.24) | 0.20 (0.15-0.26) |
| Hippocampal Tail as A3 | A1: Head | a11: Head | 0.88 (0.85-0.90) | 0.91 (0.88-0.93) |
| | A1: Head | a21: Body | 0.51 (0.47-0.56) | 0.47 (0.38-0.56) |
| | A1: Head | a31: Tail | 0.18 (0.14-0.23) | 0.12 (0.05-0.20) |
| | A2: Body | a12: Head | NA (NA-NA) | NA (NA-NA) |
| | A2: Body | a22: Body | 0.29 (0.25-0.33) | 0.39 (0.31-0.47) |
| | A2: Body | a32: Tail | 0.18 (0.13-0.24) | 0.34 (0.24-0.44) |
| | A3: Tail | a31: Head | NA (NA-NA) | NA (NA-NA) |
| | A3: Tail | a32: Body | NA (NA-NA) | NA (NA-NA) |
| | A3: Tail | a33: Tail | 0.43 (0.38-0.48) | 0.37 (0.29-0.46) |

## 2.11 Supplementary Table 11

Supplementary Table 2.11: Output from Trivariate Cholesky Model for left hemisphere using AE parameterization

| | Factor | Factor Loading | ABCD | HCP |
|---|---|---|---|---|
| Hippocampal Left Head as A3 | A1: Left Tail | a11: Left Tail | 0.73 (0.68-0.78) | 0.78 (0.71-0.83) |
| | A1: Left Tail | a21: Left Body | 0.28 (0.22-0.34) | 0.35 (0.25-0.45) |
| | A1: Left Tail | a31: Left Head | 0.18 (0.13-0.24) | 0.15 (0.07-0.24) |
| | A2: Left Body | a12: Left Tail | NA (NA-NA) | NA (NA-NA) |
| | A2: Left Body | a22: Left Body | 0.36 (0.30-0.41) | 0.39 (0.31-0.48) |
| | A2: Left Body | a32: Left Head | 0.32 (0.25-0.38) | 0.35 (0.24-0.46) |
| | A3: Left Head | a31: Left Tail | NA (NA-NA) | NA (NA-NA) |
| | A3: Left Head | a32: Left Body | NA (NA-NA) | NA (NA-NA) |
| | A3: Left Head | a33: Left Head | 0.31 (0.26-0.36) | 0.36 (0.26-0.46) |
| Hippocampal Left Body as A3 | A1: Left Head | a11: Left Head | 0.81 (0.78-0.84) | 0.86 (0.81-0.89) |
| | A1: Left Head | a21: Left Tail | 0.17 (0.12-0.22) | 0.13 (0.06-0.22) |
| | A1: Left Head | a31: Left Body | 0.39 (0.34-0.45) | 0.42 (0.32-0.51) |
| | A2: Left Tail | a12: Left Head | NA ( NA- NA) | NA (NA- NA) |
| | A2: Left Tail | a22: Left Tail | 0.57 (0.51-0.63) | 0.64 (0.55-0.73) |
| | A2: Left Tail | a32: Left Body | 0.07 (0.04-0.10) | 0.13 (0.07-0.20) |
| | A3: Left Body | a31: Left Head | NA (NA-NA) | NA (NA-NA) |
| | A3: Left Body | a32: Left Tail | NA (NA-NA) | NA (NA-NA) |
| | A3: Left Body | a33: Left Body | 0.18 (0.14-0.22) | 0.20 (0.14-0.27) |
| Hippocampal Left Tail as A3 | A1: Left Head | a11: Left Head | 0.81 (0.78-0.84) | 0.86 (0.81-0.89) |
| | A1: Left Head | a21: Left Body | 0.39 (0.34-0.45) | 0.42 (0.32-0.51) |
| | A1: Left Head | a31: Left Tail | 0.17 (0.12-0.22) | 0.13 (0.06-0.22) |
| | A2: Left Body | a12: Left Head | NA (NA-NA) | NA (NA-NA) |
| | A2: Left Body | a22: Left Body | 0.25 (0.20-0.30) | 0.33 (0.24-0.42) |
| | A2: Left Body | a32: Left Tail | 0.16 (0.10-0.23) | 0.25 (0.14-0.36) |
| | A3: Left Tail | a31: Left Head | NA (NA-NA) | NA (NA-NA) |
| | A3: Left Tail | a32: Left Body | NA (NA-NA) | NA (NA-NA) |
| | A3: Left Tail | a33: Left Tail | 0.41 (0.35-0.47) | 0.40 (0.30-0.49) |

## 2.12 Supplementary Table 12

Supplementary Table 2.12: Output from Trivariate Cholesky Model for right hemisphere using AE parameterization

| | Factor | Factor Loading | ABCD | HCP |
|---|---|---|---|---|
| Hippocampal Right Head as A3 | A1: Right Tail | a11: Right Tail | 0.70 (0.65-0.75) | 0.76 (0.69-0.82) |
| | A1: Right Tail | a21: Right Body | 0.35 (0.29-0.41) | 0.40 (0.30-0.50) |
| | A1: Right Tail | a31: Right Head | 0.17 (0.12-0.23) | 0.10 (0.04-0.19) |
| | A2: Right Body | a12: Right Tail | NA (NA-NA) | NA (NA-NA) |
| | A2: Right Body | a22: Right Body | 0.45 (0.39-0.50) | 0.46 (0.36-0.56) |
| | A2: Right Body | a32: Right Head | 0.35 (0.29-0.42) | 0.44 (0.33-0.55) |
| | A3: Right Head | a31: Right Tail | NA (NA-NA) | NA (NA-NA) |
| | A3: Right Head | a32: Right Body | NA (NA-NA) | NA (NA-NA) |
| | A3: Right Head | a33: Right Head | 0.30 (0.26-0.35) | 0.33 (0.25-0.42) |
| Hippocampal Right Body as A3 | A1: Right Head | a11: Right Head | 0.83 (0.79-0.86) | 0.87 (0.83-0.90) |
| | A1: Right Head | a21: Right Tail | 0.14 (0.10-0.19) | 0.09 (0.03-0.16) |
| | A1: Right Head | a31: Right Body | 0.50 (0.45-0.55) | 0.49 (0.39-0.57) |
| | A2: Right Tail | a12: Right Head | NA (NA-NA) | NA (NA-NA) |
| | A2: Right Tail | a22: Right Tail | 0.56 (0.50-0.62) | 0.67 (0.58-0.75) |
| | A2: Right Tail | a32: Right Body | 0.09 (0.06-0.13) | 0.18 (0.11-0.25) |
| | A3: Right Body | a31: Right Head | NA (NA-NA) | NA (NA-NA) |
| | A3: Right Body | a32: Right Tail | NA (NA-NA) | NA (NA-NA) |
| | A3: Right Body | a33: Right Body | 0.21 (0.17-0.24) | 0.20 (0.14-0.26) |
| Hippocampal Right Tail as A3 | A1: Right Head | a11: Right Head | 0.83 (0.79-0.86) | 0.87 (0.83-0.90) |
| | A1: Right Head | a21: Right Body | 0.50 (0.45-0.55) | 0.49 (0.39-0.57) |
| | A1: Right Head | a31: Right Tail | 0.14 (0.10-0.19) | 0.09 (0.03-0.16) |
| | A2: Right Body | a12: Right Head | NA (NA-NA) | NA (NA-NA) |
| | A2: Right Body | a22: Right Body | 0.30 (0.26-0.34) | 0.37 (0.29-0.46) |
| | A2: Right Body | a32: Right Tail | 0.18 (0.12-0.23) | 0.32 (0.22-0.43) |
| | A3: Right Tail | a31: Right Head | NA (NA-NA) | NA (NA-NA) |
| | A3: Right Tail | a32: Right Body | NA (NA-NA) | NA (NA-NA) |
| | A3: Right Tail | a33: Right Tail | 0.38 (0.32-0.44) | 0.35 (0.26-0.45) |

## 2.13 Supplementary Table 13

Supplementary Table 2.13: Phenotypic correlations for both ABCD and HCP samples

| Brain Region | ABCD | | HCP | |
|---|---|---|---|---|
| | $MZ_r$ | $DZ_r$ | $MZ_r$ | $DZ_r$ |
| Total Brain Volume | 0.95 | 0.56 | 0.92 | 0.53 |
| Whole Hippocampus | 0.88 | 0.48 | 0.92 | 0.44 |
| Hippocampal Head | 0.87 | 0.50 | 0.91 | 0.47 |
| Hippocampal Body | 0.80 | 0.42 | 0.87 | 0.37 |
| Hippocampal Tail | 0.80 | 0.34 | 0.82 | 0.42 |
| Posterior Hippocampus | 0.83 | 0.40 | 0.88 | 0.37 |
| Subiculum | 0.86 | 0.45 | 0.85 | 0.40 |
| CA1 | 0.85 | 0.55 | 0.86 | 0.38 |
| Hippocampal Fissure | 0.52 | 0.27 | 0.66 | 0.22 |
| Presubiculum | 0.78 | 0.41 | 0.76 | 0.45 |
| Parasubiculum | 0.58 | 0.26 | 0.67 | 0.31 |
| GC-ML-DG | 0.83 | 0.52 | 0.85 | 0.34 |
| CA3 | 0.70 | 0.37 | 0.73 | 0.33 |
| CA4 | 0.83 | 0.51 | 0.85 | 0.30 |
| Fimbria | 0.68 | 0.35 | 0.61 | 0.41 |
| Hippocampal-Amygdala-Transition-Area | 0.67 | 0.33 | 0.72 | 0.57 |